약학박사학위논문

인터페론 베타 기반 항암 치료법 연구

The Study for Interferonβ-1a-based Anti-cancer Therapeutics

2017 년 2 월

서울대학교 대학원
약학과 병태생리학 전공
김 태 은

Abstract

The Study for Interferonβ-1a-based Anti-cancer Therapeutics

Tae-Eun Kim
College of Pharmacy
The Graduate School
Seoul National University

Interferonβ (IFNβ) has recently emerged as an anti-cancer drug owing to its ability to preferentially induce apoptosis in cancer cells. However, IFNβ resistance, the low stability and systemic toxicity of its derivative agents limit its use in treating cancer. Previously a glycoengineered version of recombinant human IFNβ-1a, termed R27T was developed which has two N-glycosylation sites: one at the 80th amino acid (original site) and one at the 25th amino acid (additional site). Compared to the parent molecule, R27T exhibited superior stability, solubility, productivity, and pharmacokinetic properties without any loss of biological activity and change in receptor-binding affinity. However, R27T alone, like its parental molecule, still has significant issues with resistance and toxicity.

In this study, I first examined the anti-cancer efficacy of R27T in various cancer cells. I found that its decreased ability to induce anti-proliferation and apoptosis in resistant cells was due to an upregulation of cellular FLICE-like inhibitory protein (cFLIP), which impairs caspase activation. I thus investigated whether inhibition of cFLIP could facilitate R27T-induced caspase activation. Toward this end, I evaluated the abilities of a cFLIP small interfering RNA (siRNA) or 4,5,6,7-tetrabromobenzotriazole [TBB, a casein kinase-2 (CK-2) inhibitor] to enhance the anti-cancer effects of R27T *in vitro* and *in vivo*.

To support the further application of R27T, I developed a fusion protein in which R27T was fused to the C-terminus of the heavy chain of a trastuzumab, an anti-ERBB-2 antibody and assessed its potential for treating ERBB-2+ gastric cancer. R27T fused protein exhibited a higher expression level in CHO cells compared with that of the parental IFNβ-1a fused protein. The fusion protein induced IFN signaling in gastric cancer cells exhibiting direct anti-cancer efficacy. Moreover, I have verified the antibody-dependent cellular cytotoxicity and complement dependent cytotoxicity using fusion protein in gastric cancer cells.

Keywords: recombinant human interferonβ-1a, R27T, anti-cancer, resistance, cFLIP, trastuzumab, fusion protein

Student Number: 2011-31101

Contents

Abstract ····· **i**

Contents ····· **iii**

List of Tables ····· **v**

List of Figures ····· **vi**

List of Abbreviations ····· **x**

I. Introduction

1. Type I interferons ····· 2

1.1 Type I interferon for cancer therapy ····· 2

1.2 Type I interferon resistance in cancer ····· 6

1.3 Type I interferon combination therapy for cancer ····· 8

2. Cellular FLICE inhibitory protein in cancer ····· 10

2.1 Isoforms of cFLIP ····· 10

2.2 Functions of cFLIP ····· 12

3. Antibody-cytokine fusion protein for cancer therapy ····· 15

II. Purpose of the study ····· **17**

III. Part I. Sensitization of glycoengineered interferonβ-1a-mutein resistant cancer cells by cFLIP inhibition for enhanced anti-cancer therapy

Introduction ····· 21

Materials and methods ····· 23
Results ····· 32
Discussion ····· 63
VI. Part II. The development anti-ERBB-2 antibody-glycoengineered interferonβ-1a mutein fusion protein for gastric cancer therapy
Introduction ····· 69
Materials and methods ····· 73
Results ····· 79
Discussion ····· 98
VII. Conclusion and perspectives ····· 101
References ····· 106
국문 초록 ····· 127

List of Tables

Introduction

Table 1. Deregulation of various IFN signaling components

Table 2. Antibody-cytokine fusion proteins in clinical development

Part II

Table 1. Properties of cytokines under evaluation for cancer immunotherapy

List of Figures

Introduction

Figure 1. Type 1 interferon-induced signaling and transcription

Figure 2. Structures of cFLIP isoforms

Figure 3. cFLIP mediated inhibition of caspase-8 activation.

Figure 4. Analysis of cFLIP expression level data from the cBioPortal database

Part I

Figure 1. Analysis of anti-proliferative effects of R27T in different cell lines by WST assay

Figure 2. Analysis of anti-proliferative effects of R27T in different cell lines by live cell imaging

Figure 3. Pro-apoptotic effects of R27T in different cell lines

Figure 4. Ability of R27T to induce the IFN signaling

Figure 5. Ability of R27T to increase the mRNA expression of apoptotic mediators

Figure 6. Ability of R27T to increase the protein expression of apoptotic

mediators

Figure 7. Ability of R27T to activate the caspase-8

Figure 8. Ability of R27T to activate the caspase cascade and cFLIP expression

Figure 9. cFLIP expression in R27T-sensitive and -resistant cancer cells

Figure 10. Activation of NF-κB p65 and NFAT1c by R27T treatment

Figure 11. Inhibition of anti-proliferation efficacy of R27T by co-treatment with zVAD

Figure 12. Inhibition of anti-proliferation efficacy of R27T by cFLIPS expression

Figure 13. Inhibition of cFLIP expression with siRNA enhances caspase-8 activation in R27T-resistant cells

Figure 14. Inhibition of cFLIP expression with TBB enhances caspase-8 activation in R27T-resistant cells

Figure 15. TBB-mediated reduction of cFLIP

Figure 16. Inhibition of cFLIP expression with siRNA enhances R27T-induced anti-proliferation and apoptosis in R27T-resistant cells

Figure 17. Inhibition of cFLIP expression with TBB enhances R27T-induced anti-proliferation and apoptosis in R27T-resistant cells

Figure 18. Restoration of cFLIP by expression vector transfection prior to TBB or R27T treatment

Figure 19. *In vivo* anti-tumor efficacy of R27T in OVCAR-3 xenograft mouse model

Figure 20. *In vivo* anti-tumor efficacy of co-treatment with R27T plus TBB in HeLa xenograft mouse model

Figure 21. Immunohistochemical detection of cFLIP in HeLa tumor xenografts

Part II

Figure 1. Schematics of trastuzumab-R27T and its constituents

Figure 2. Purification of trastuzumab-R27T

Figure 3. Comparison of expression level between trastuzumab-IFNβ-1a and trastuzumab-R27T

Figure 4. Size analysis of trastuzumab-R27T

Figure 5. Structural analysis of trastuzumab-R27T

Figure 6. IFN functions of trastuzumab-R27T

Figure 7. Analysis of ERBB-2-targeting function by FACS

Figure 8. Analysis of ERBB-2-targeting function by confocal microscopy

Figure 9. *In vitro* direct anti-cancer efficacy of trastuzumab-R27T

Figure 10. *In vitro* CDC efficacy of trastuzumab-R27T

Figure 11. *In vitro* ADCC efficacy of trastuzumab-R27T

Conclusion and perspectives

Figure 1. Strategy for combination therapy

List of Abbreviations

Abbreviation	Word
ADCC	antibody-dependent cellular cytotoxicity
CD	circular dichroism
CDC	complement dependent cytotoxicity
cFLIP	cellular FLICE-like inhibitory protein
cFLIPL	cFLIP-long
cFLIPS	cFLIP-short
CK-2	casein kinase-2
DAPI	4,6-diamidino-2-phenylindole dihydrochloride
EGFR	epidermal growth factor receptor
ERBB-2	epidermal growth factor receptor-2
HUVECs	human umbilical vein endothelial cells
IFN	interferon
IFNAR1	interferon-alpha/beta receptor alpha chain
IFNAR2	interferon-alpha/beta receptor beta chain

IL-2	interleukin-2
IRDS	IFN-related DNA damage-resistant signature
ISGF3	interferon-stimulated gene factor 3
ISREs	IFN-stimulated regulatory elements
NK	natural killer
PD-1	programmed cell death protein 1
PD-L1	programmed death-ligand 1
rhIFN	recombinant human interferon
RP-HPLC	reverse phase-high performance liquid chromatography
siRNA	small interfering RNA
STAT	signal transducers and activator of transcription
TBB	4,5,6,7-tetrabromobenzotriazole
U-STAT	unphosphorylated STAT
U-ISGF3	unphosphorylated ISGF3
WST	water-soluble tetrazolium

Introduction

1. Type I interferons

1.1 Type I interferon for cancer therapy

The interferon (IFN) family cytokines can be classified into two major groups: type I (predominantly α or β) and type II (γ) [1]. The type I IFNs exhibit their effects by binding a heterodimer cell surface receptor that consists of IFNAR1 (Interferon-alpha/beta receptor alpha chain) and IFNAR2 (Interferon alpha/beta receptor beta chain). Following the binding of type I IFN to this receptor, Janus kinases phosphorylate the signal transducers and activator of transcription (STAT) proteins are activated. A ternary complex, interferon-stimulated gene factor 3 (ISGF3), that includes phosphorylated STAT-1, -2 and IRF9, translocate into the nucleus and binds to IFN-stimulated regulatory elements (ISREs), leading to the transcription of IFN-stimulated genes [2]. These genes mediate pleiotropic biological activities, including anti-viral [3], anti-proliferative [4], anti-angiogenic [5], and immunomodulatory [6] processes (Figure 1).

The type I IFNs are also involved in cell differentiation and anti-cancer activity. There are several mechanisms underlying the anti-cancer effects of type I IFNs. They have direct effects, such as the induction of apoptosis and blockade of the cell cycle. The initiation of apoptosis can act through an extrinsic pathway (e.g., the activation of the death receptors), via an intrinsic and/or mitochondrial pathway, or by the stress kinase cascade [7-10]. In

addition to these direct effects, type I IFNs also have several indirect anti-cancer effects, such as inducing immunomodulatory functions (e.g., the activation of cytotoxic T-lymphocytes, natural killer (NK)-cells, and monocytes [11]) and enhancing the cell-surface expression of class I major histocompatibility complex antigens [12, 13]. Furthermore, several non-immunomodulatory host effects of type I IFNs, such as the inhibition of the transcription/secretion of anti-angiogenic factors [14-16] and the down-regulation of interactions between tumors and the surrounding stroma [17], have been demonstrated.

Most of the clinical trials of IFNs in cancer therapy have involved type I IFNs. They demonstrated efficacy against certain types of cancers in early trials, and have been approved for the treatment of hairy cell leukemia, chronic myelogenous leukemia, Kaposi's sarcoma, melanoma, and renal cell carcinoma [18, 19]. However, the use of IFNs in cancer therapy has declined in recent years due to the systemic toxicity associated with IFN and the development of more effective therapeutics with lower side effects. Because of the proven anti-cancer effects of type I IFN, however, novel therapeutic strategies using this agent are continually being developed by many research groups [20].

Accruing evidence suggests that the efficacies of chemotherapeutics, targeted anti-cancer therapeutics, radiotherapy, and immunotherapy depend on type I IFN-mediated signaling [20]. In *in vivo* mouse models, for example,

anti-IFNAR1 antibodies blocked the anti-tumor effect of monoclonal antibodies targeting human epidermal growth factor receptor 2 (ERBB2) or epidermal growth factor receptor (EGFR) [21, 22]. The effect of anthracycline-based chemotherapy in cancer-cell-xenografted mice was also inhibited by co-treatment of an anti-IFNAR1 monoclonal antibody [23].

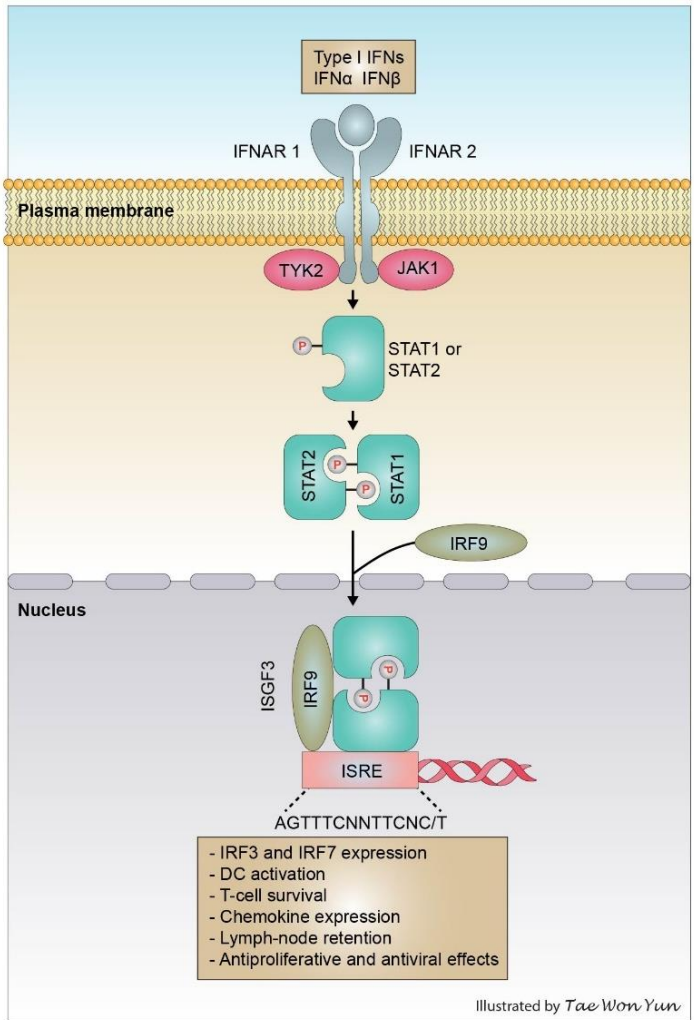

Figure 1. Type I interferon-induced signaling and transcription. Receptor binding of type I IFNs induces STAT-1/-2 phosphorylation through the receptor associated JAK1. The phosphorylated STAT-1/-2 form a complex with IRF-9. The STAT-1/-2-IRF-9 complex (ISGF3) regulates expression of genes with ISREs in their promoters.

1.2 Type I interferon resistance in cancer

As IFNs are strong suppressors of growth, tumor cells with truncated, restrained, or dysfunctional IFN signaling components can evade the effects of endogenous IFN and the innate immune response, and thus exhibit increased proliferation. Such a view is supported by studies showing that cells with dysfunctional type I and type II IFN signaling components are more susceptible to spontaneous and induced tumor formation [24-28]. Moreover, many malignancies are reportedly associated with deregulated/resistant IFN-signaling pathways.

There are several issues should be considered in developing type I IFN based anti-cancer therapeutics. One of them is the production of U-STAT, which is known to be produced under the chronic exposure to low levels of endogenous type I IFN. U-STAT1, together with U-STAT2 and IRF9, forms an unphosphorylated ISGF3 (U-ISGF3) and increased U-ISGF3 levels lead to enhanced expression of IFN-related DNA damage-resistant signature (IRDS) inhibiting increase of other ISGs that are related to anti-proliferative or pro-apoptotic responses [29, 30].

The possible deregulations of various IFN signaling components in malignant and IFN-resistant cells are listed in Table 1.

Table 1. Deregulation of various IFN signaling components

Signaling stage	Mechanism	Reference
Receptor	Receptor low expression	[31]
	Receptor mutation	[32]
	Soluble receptor presence in serum	[33, 34]
JAK-STAT	JAK1 mutation	[35-37]
	STAT expression/activation	[38, 39]
	U-STAT1/2	[30]
	SOCS expression	[40]
Transcriptional	ISGF3 component deficiency	[41]

1.3 Type I interferon combination therapy for cancer

The existing literature clearly shows that co-treatment with IFNs plus other strategies, including chemotherapeutics, hormones, radiotherapy, and other immunostimulatory molecules, is effective against cancer [42]. A combination regimen of IFN plus chemotherapeutics triggers cancer cell death in proliferating cells while stimulating an IFN-induced immune response [43]. The IFN signaling pathway has been reported to enhance the effects of chemotherapeutics in mouse models of breast cancer, supporting the benefit of combination therapy with IFN and chemotherapeutics in patients [23]. IFN has also been shown to stimulate the anti-cancer effects of ERBB-2-targeting drugs, such as trastuzumab and lapatinib, potentially via a mechanism that requires both type I and type II IFN immune stimulatory responses [21, 44].

Tumor cells can both directly and indirectly suppress the anti-tumor immune response [45], such as via the suppressive microenvironment of large primary or metastatic tumors, and through the expression of ligands that target inhibitory receptors (e.g., programmed cell death protein 1 (PD-1) or cytotoxic T-lymphocyte-associated protein 4) on immune effector cells to inactivate an anti-tumor immune response [46]. As radiotherapy can reportedly moderate the immuno‑suppressed tumor microenvironment [47], it has been proposed that a combined regimen of radiotherapy plus an immune-stimulating agent, such as IFN, could reactivate the anti-tumor

immune response [48]. Interestingly, IFN treatment was reported to induce the expression of programmed death-ligand 1 (PD-L1), which can suppress anti-tumor immune responses [49]. Therefore, combined therapies involving IFN plus PD1-PD-L1 blockers could be effective.

2. Cellular FLICE inhibitory protein in cancer

2.1 Isoforms of cFLIP

Cellular FLICE inhibitory protein (cFLIP), also known as CFLAR, Casper, iFLICE, FLAME-1, CASJ, CLARP, MRIT or usurpin, is a pivotal negative regulator of the apoptotic signaling pathway [50]. Currently, 15 different variants have been identified, but only 3 of these, cFLIPL, cFLIPS, and cFLIPR, have been shown to be translated to protein (Figure 2). The 55kDa protein cFLIPL is structurally similar to procaspase-8 which has two N-terminal DED domains and a C-terminal caspase-like domain [51]. The C-terminal domain of cFLIPL lacks the catalytic cysteine residue, which cleaves caspases. Thus, cFLIPL has lack of enzymatic activity. c-FLIPS (26 kDa) and cFLIPR (24 kDa) also contain two N-terminal DED domains, but contain a shorter carboxyl terminus than cFLIPL [52]. All three isoforms of cFLIP can be recruited to the DISC through an interaction of their double DED domains with the adaptor protein FADD.

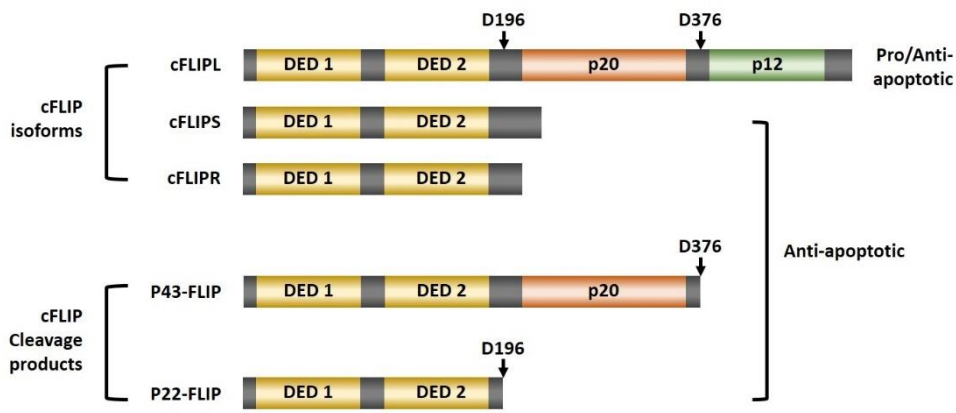

Figure 2. Structures of cFLIP isoforms. Three cFLIP isoforms, cFLIPL, cFLIPS, and cFLIPR, contain tandem death effector domains (DED 1/2) at their N-terminus. In addition to tandem DED 1/2, cFLIPL possesses a caspase-like domain without catalytic activity.

2.2 Functions of cFLIP

Recruitment of cFLIPS to the death-inducing signaling complex (DISC) impedes procaspase-8 homo-dimerization and activation, inhibiting the activation of the apoptotic caspase cascade. cFLIPL, whereas forms a hetero-dimeric complex with caspase-8, but unlike cFLIPS, hetero-dimerization of cFLIPL and procaspase-8 allows activation of caspase-8 through its self-cleavage [53]. As a result of limited caspase-8 activation, the p43-cFLIP and the p41/43 caspase-8 subunits are generated. However, due to the absence of proteolytic activity of cFLIPL, no further processing is triggered. Thus cleaved caspase-8 and cFLIPL are remained at the DISC, blocking additional transduction of the apoptotic signaling (Figure 3) [54].

The elevated expression level of cFLIP has been found in various cancer types. Several studies with cancer cell lines have demonstrated increased cFLIP expression levels in colorectal cancer [55], pancreatic cancer [56], gastric cancer [57], ovarian cancer [58], prostate cancer [59], and melanoma. cFLIP was also expressed at high level in primary tissues from patients with bladder cancer [60, 61], lung cancer [62, 63], liver cancer [64], gastric cancer [65, 66], and melanoma [67]. Overexpression of cFLIP is related with a resistance to Fas and TRAIL mediated apoptosis. Moreover, Djerbi et al. reported that high levels of cFLIP expression in some tissue types are correlated with tumor aggressiveness [68]. The levels of cFLIP gene expression in human cancers are displayed in Figure 4.

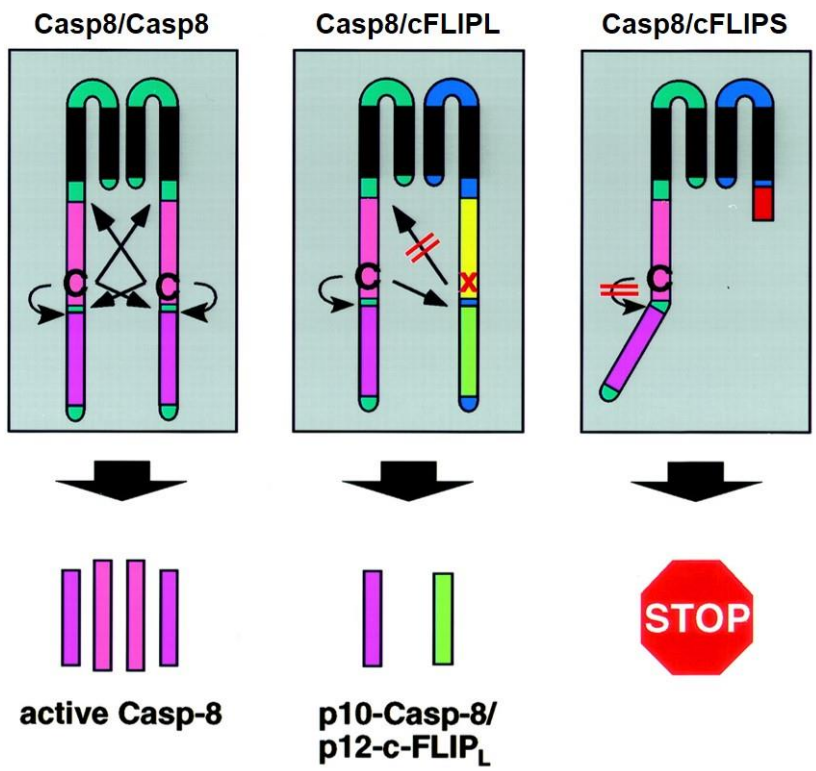

Figure 3. cFLIP mediated inhibition of caspase-8 activation. cFLIPL forms hetero-dimers with caspase-8, partially inhibiting caspase-8 activation. When caspase-8 form a complex with cFLIPS, caspase-8 remains uncleaved (non-funtional). Source of figure : Krueger A, 2001 [54].

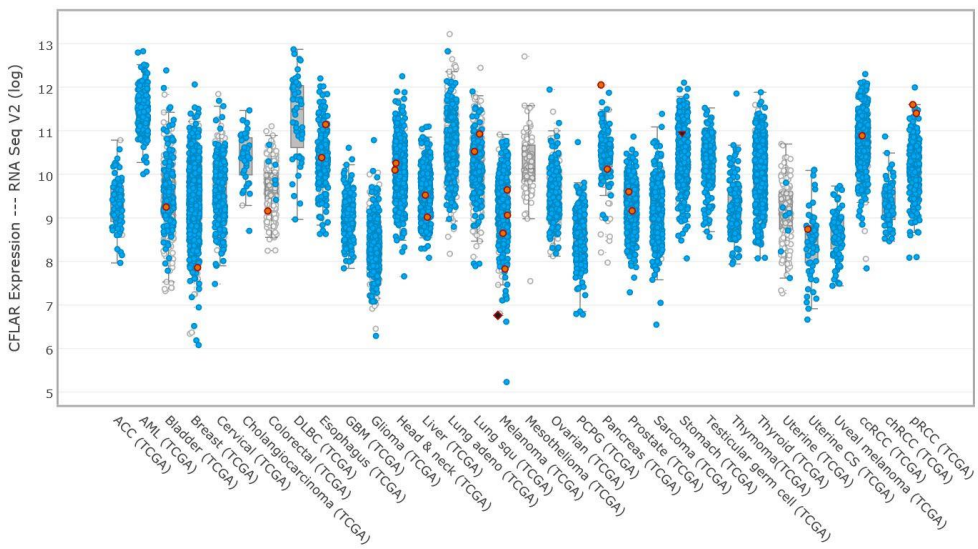

Figure 4. Analysis of cFLIP expression level data from the cBioPortal database (http://www.cbioportal.org/index.do). Every spot represents a single study. White spots represent those analyzed without gene sequencing, blue spots represent normal results of gene sequencing, red spots represent missense mutations, diamond spots represent nonsense mutations, and inverted triangles represent frameshift mutations.

3. Antibody-cytokine fusion protein for cancer therapy

Cytokines are the major regulators of the immune system and released by various cell types including immune cells. Secreted cytokines could activate innate and adaptive immune responses and affect cell proliferation, differentiation, effector functions, and survival [69]. For its ability in activation of immune response toward to cancer cells, cytokine have been extensively studied for cancer therapy [70]. Several cytokines including interleukin-2 (IL-2), other members of common gamma chain cytokine family (IL-7, IL-15, IL-21), IL-12, and the interferons (IFNs), have been reported to exhibit anti-cancer efficacy [71-73]. However, therapies using cytokine alone induce severe side effect, such as systemic inflammation or vascular leak syndrome [74]. These side effects are resulted from absorption of cytokine in the peripheral tissues prior to reaching the tumor site. Because the cytokines could not be specifically transported to tumor site, high doses of cytokines need to be injected to induce sufficient anti-cancer efficacy, which induces unwanted toxicity. Currently, the development of recombinant antibody technologies enables the creation of antibody-cytokine fusion proteins [75]. These fusion proteins utilize the tumor-targeting ability of monoclonal antibodies to lead cytokines specifically to tumor tissue allowing them stimulate more enhanced anti-tumor immune responses while mitigating the systemic toxicities [76-78]. The antibody-cytokine fusion proteins under clinical development are listed in Table 2.

Table 2. Antibody-cytokine fusion proteins in clinical development

Fusion Protein	Company	Antigen	Structure	Clinical Stage	Ref.
Hu 14.18-IL2	Merck KGaA	GD2	IgG	Phase II	[79-82]
DI-Leu16-IL2	Alopexx Oncology	CD20	IgG	Phase I/II	[83]
Anti-CD20 tetrameric hIFNα	Immunomedics	CD20	IgG	Preclinical	[84]
Anti-CD20-IFNα	Immungene	CD20	IgG	Pre-phase I	[85]
Anti-CD20-IL-21	none	CD20	IgG	Preclinical	[86]
Anti-HLA-DR-tetrameric IFNα-2b	Immunomedics	HLA-DR	IgG	Preclinical	[87]
NHS-IL2LT	Merck KGaA	DNA	IgG	Phase I	[88, 89]
NHS-IL12	Merck KGaA	DNA	IgG	Phase I	[90]
F16-IL2	Philogen	A1 domain of Tenascin C	Diabody	Phase Ib/II	[91-93]
L19-IL2	Philogen	ED-B Fibronectin	Diabody	Phase II	[94-96]
L19-TNFα	Philogen	ED-B Fibronectin	Diabody	Phase I/II	[97-99]
huBC1-IL12	Antisoma	ED-B Fibronectin	IgG	Phase I/II	[100, 101]
huKS-IL2	Seono	EpCAM	IgG	Phase I/II	[102, 103]
Anti-CEA-IL2v	Roche	Carcinoembryonic antigen	IgG	Phase I	[104]
BC1-IL12	Antisoma	ED-B variant of fibronectin	IgG	Phase I	[101]

Purpose of the study

Interferonβ (IFNβ) has recently emerged as an anti-cancer drug owing to its ability to preferentially induce apoptosis in cancer cells. However, resistance, toxicity, and high price has limited the usefulness of IFNβ to treat cancer. Previously, a glycoengineered version of recombinant human IFNβ-1a, termed R27T was developed. This agent has two N-glycosylation sites: the original site at the 80th amino acid, plus an additional site at the 25th amino acid, which was induced by mutating an arginine to a threonine at the 27th position. R27T exhibited superior stability, solubility, productivity, and pharmacokinetic properties without any loss of biological activity or alteration of receptor binding affinity, relative to those of its parental molecule. Although the protein stability is improved, it still has a resistance and toxicity problem.

The therapies using cytokine alone induce severe side effect, such as systemic inflammation or vascular leak syndrome. These side effects are resulted from absorption of cytokine in the peripheral tissues on the way to reach tumor site. Because the cytokines could not be specifically transported to tumor site, high doses of cytokines need to be injected to display anti-cancer efficacy, which induces unwanted toxicity. In the same manner, the therapeutic use of free IFNs has been limited by a dose-limiting systemic toxicity that makes it impossible deliver optimal concentrations deep into tumor tissues, thus the true therapeutic potential of IFN has not been fully exploited.

The purpose of this study is twofold: firstly, to examine the molecular mechanism underlying the resistance of cancer cells to R27T and sought to overcome R27T resistance through combination therapy, and secondly, to reduce R27T toxicity, monoclonal antibody-R27T fusion protein was developed and its bioactivity and therapeutic efficacy was confirmed.

PART I

Sensitization of glycoengineered interferonβ-1a-mutein resistant cancer cells by cFLIP inhibition for enhanced anti-cancer therapy

Introduction

Interferonβ (IFNβ) has emerged as a potential anti-cancer drug that can effectively induce cancer growth arrest by decreasing cell proliferation and inducing apoptosis [105]. However, the use of IFNβ in anti-cancer therapy has been hampered by its low stability and relatively short circulating half-life (3-5 h in humans) [106].

In a previous study, R27T, a glycoengineered version of recombinant human IFNβ-1a was developed. R27T has two N-glycosylation sites: at the 80^{th} amino acid (the original site) and an additional site at the 25^{th} amino acid, induced by mutating an arginine to threonine at the 27^{th} position [107]. R27T exhibited superior stability, solubility, productivity, and pharmacokinetic properties without any loss of biological activity or alteration of receptor binding affinity, compared to those of its parent molecule, IFNβ-1a. However, the anti-cancer efficacy of R27T has not yet been fully explored. In addition, IFNβ resistance reportedly develops in diverse tumor cells via deregulation of the IFNβ signaling pathway [108-110]. Therefore, I need to explore additional approaches, such as combination therapy, as a means to enhance the therapeutic efficacy of R27T.

In this study, the anti-cancer efficacy of R27T was first examined in various cancer cells. I found that the resistance to R27T-induced anti-proliferation and apoptosis was due to the increased expression of cellular

FLICE-like inhibitory protein (cFLIP), which blocks the initiation of caspase activation. I investigated whether the inhibition of cFLIP could facilitate R27T-induced caspase activation. Therefore, I evaluated the ability of cFLIP small interfering RNA (siRNA) or 4,5,6,7-tetrabromobenzotriazole (TBB, a casein kinase-2 [CK-2] inhibitor) to enhance the anti-cancer effects of R27T *in vitro* and *in vivo*.

Materials and methods

1. Construction of plasmids

In order to establish a cell line that transiently express cFLIP-short (cFLIPS), pCMV3-cFLIPS was constructed. The cFLIPS gene synthesized by Bioneer (Daejeon, Korea) was excised with KpnI (Thermo Scientific, Pittsburgh, PA, USA) and XbaI (Thermo Scientific) and inserted to pCMV3. The pCMV-cFLIP-long (cFLIPL) was purchased by Sino Biological (Beijing, China).

2. Cell lines and culture condition

Human ovarian carcinoma (OVCAR-3, TOV-21G), human cervical cancer (HeLa), and human breast cancer (MCF-7) cell lines were purchased from the American Type Culture Collection (ATCC; Manassas, VA, USA). OVCAR-3, HeLa, and MCF-7 cells were cultured in RPMI-1640 (HyClone, Logan, UT, USA) supplemented with 10% fetal bovine serum (HyClone), 100 units/mL penicillin, and 100 μg/mL streptomycin (HyClone). TOV-21G cells were maintained in a 1:1 mixture of M199/MCDB medium (HyClone) containing 15% fetal bovine serum, 100 units/mL penicillin, and 100 μg/mL streptomycin. All cells were grown at 37ºC in a humidified 5% CO_2 atmosphere

3. Cell viability and apoptosis assays

The *in vitro* anti-proliferation efficacy of R27T (provided from Abion Inc. [107]) was tested using two different cell viability assays. . OVCAR-3, MCF-7, HeLa, or TOV-21G cells were seeded in 96-well plates, cultured overnight, and then treated with or without various concentrations of R27T for 24, 48, or 72 h. For combination treatment, OVCAR-3 or HeLa cells were treated with R27T (100 ng/mL), zVAD (50 μM; R&D Systems, Minneapolis, MN, USA), and/or TBB (10 μM; Tocris Bioscience, Bristol, UK), alone or in combination, for 48 or 72 h. ON-TARGET plus human cFLIP siRNA set was supplied by Dharmacon (Lafayette, CO, US). The sequences of siRNAs used for transfection were as follows: 5'-GUGCCGGGAUGUUGCUAUA-3' (sense) and 5'- UAUAGCAACAUCCCGGCAC-3' (antisense); 5'-CAAGCAGUCUGUUCAAGGA-3' (sense) and 5'-UCCUUGAACAGACUGCUUG-3' (antisense); 5'-CAUGGUAUAUCCCAGAUUC-3' (sense) and 5'-GAAUCUGGGAUAUACCAUG-3' (antisense); 5'-CCUAGGAAUCUGCCUGAUA-3' (sense) and 5'-UAUCAGGCAGAUUCCUAGG-3' (antisense). For sequential treatment with R27T and cFLIP siRNA, HeLa cells were transfected with 10 nM of scrambled siRNA (Dharmacon) or cFLIP siRNA for 24 h. Thereafter, the siRNA-containing culture medium was removed and cells were cultured in fresh medium containing R27T (100 ng/mL). Cell viability was assessed

using a water-soluble tetrazolium (WST) colorimetric assay (Ez-Cytox; Daeil Lab Service, Seoul, Korea) or a live cell-staining assay (LIVE/DEAD Viability Assay; Molecular Probes, Eugene, OR, USA). For the WST assay, 10 μL of WST reagent was added to each well, the plates were incubated for 1 h, and absorbance was measured at 430 nm using a microplate reader (TECAN, Durham, NC, USA). For live-cell analysis, calcein-AM was treated to cells for 10 min and the fluorescence of calcein-AM (which is specifically taken up by live cells) was analyzed using a fluorescence microscope (Leica, Wetzlar, Germany).

R27T-induced apoptosis was measured using a fluorescence isothiocyanate (FITC) Annexin V/PI kit (BD Bioscience, San Jose, CA, USA). Annexin V can detect apoptotic cells by binding to phosphatidylserine and PI is used for nuclear DNA staining. Cells are Annexin V positive and PI negative in early apoptosis, while cells are both Annexin V and PI positive in late apoptosis [111]. Briefly, cells were harvested, washed twice with phosphate-buffered saline (PBS), and resuspended in 100 μL of binding buffer (10 mM HEPES/NaOH [pH 7.4], 140 mM NaCl, and 2.5 mM $CaCl_2$). Five microliters of FITC Annexin V or PI solution were added to each sample, and the samples were incubated for 15 min at room temperature in the dark. The reaction was stopped by adding 400 μL of binding buffer. The stained samples were run on a FACSCalibur flow cytometer (BD Biosciences) and analyzed with the Cell QuestPro (BD Biosciences).

4. Luciferase reporter assay

Reporter gene assays were performed using a Dual Luciferase Assay kit (Promega, Madison, WI, USA). OVACAR-3 or HeLa cells were seeded to 12-well plates and incubated overnight at 37°C in a humidified atmosphere containing 5% CO_2. The cells were then co-transfected with 0.4 μg of a firefly luciferase-encoding reporter plasmid containing the interferon stimulated response element (ISRE) and 0.3 μg of pTK-RLuc plasmid containing the *Renilla* luciferase reporter gene. Transfections were performed with the Lipofectamine LTX reagent (Invitrogen, Carlsbad, CA, USA). At 24 h post-transfection, cells were treated with the indicated concentrations of R27T, and after an additional 16 h, the activities of firefly luciferase and *Renilla* luciferase were determined using a microplate reader (TECAN).

5. Quantitative real-time reverse transcription-polymerase chain reaction (qRT-PCR)

OVCAR-3 or HeLa cells were treated with 100 ng/mL R27T, total RNA was isolated using a Hybrid-RTM kit (GeneAll, Seoul, Korea), and the RNA was reverse transcribed to complementary DNA (cDNA) using a Transcriptor First Strand cDNA synthesis kit (Roche, Indianapolis, IN, USA). TaqMan qRT-PCR was performed using the following primers and probes: death receptor 4 (DR4; forward primer, 5'-GGGTCCACAAGACCTTCAAGT-3'; reverse primer, 5'-TGCAGCTGAGCTAGGTACGA-3'; and probe, 5'-FAM-

TCCTGCTG-TAMRA-3'), FAS (forward primer, 5'-ATGGCCAATTCTGCCATAAG-3'; reverse primer, 5'-TGACTGTGCAGTCCCTAGCTT-3'; and probe, 5'-FAM-TCCTCCAG-TAMRA-3'), tumor necrosis factor alpha (TNF-α; forward primer, 5'-GACAAGCCTGTAGCCCATGT-3'; reverse primer, 5'-TCTCAGCTCCACGCCATT-3'; and probe, 5'-FAM-CCTCCTGG-TAMRA-3'), and TNF-related apoptosis-inducing ligand (TRAIL; forward primer, 5'-CCTCAGAGAGTAGCAGCTCACA-3'; reverse primer, 5'-CAGAGCCTTTTCATTCTTGGA-3'; and probe, 5'-FAM-CAGAGGAA-TAMRA-3'). The following cycling conditions were applied: 95°C for 10 min; followed by 50 cycles of 95°C for 10 s and 55°C for 30 s; and a final cycle at 40°C for 30 s. The primers and probes were designed by the Universal Probe Library Assay Design Center (Roche Diagnostics, Basel, Switzerland), and qRT-PCR was performed on a LightCycler 2.0 (Roche Diagnostics, Mannheim, Germany). The 2(-ΔΔC(T)) method was used to compute relative mRNA expression levels [112].

6. Antibodies and Western blot analysis

OVCAR-3 or HeLa cells treated with R27T (100 ng/mL), cFLIP siRNA (10 nM), and/or TBB (10 μM), alone or in combination, were lysed in RIPA lysis buffer (150 mM sodium chloride, 1% Triton X-100, 1% sodium deoxycholate, 0.1% SDS, 50 mM Tris-HCl [pH 7.5], 2 mM EDTA)

supplemented with a protease inhibitor mixture (Roche). The lysed cells were incubated for 20 min on ice and clarified by centrifugation at 12,000 × g for 15 min. The supernatant was collected, and protein concentration was determined using a BCA protein assay kit (Thermo Scientific) according to the manufacturer's instructions. Twenty micrograms of protein were resolved by 12% SDS-PAGE and transferred to a polyvinyl difluoride membrane (PVDF; BioRad, CA, USA). The PVDF membranes were blocked in TBS-Tween20 buffer containing 5% skim milk and incubated with primary antibodies at 4°C overnight. The following primary antibodies were utilized: anti-FAS, anti-TNF-α, anti-TRAIL, anti-caspase-8, anti-caspase-3, anti-caspase-9, anti-p65, anti-p-p65 (all from Cell Signaling Technology, Danvers, MA, USA), anti-cFLIPS (AG Scientific, CA, USA), anti-DR4 (Abcam, Cambridge, UK), anti-cFLIPL, anti-nuclear factor of activated T-cells 1c (NFAT1c) and anti-β-actin (both from Santa Cruz Biotechnology, Santa Cruz, CA, USA). The blots were then incubated for 1 h with anti-mouse IgG-HRP (ThermoFisher Scientific) or anti-rabbit IgG-HRP (ThermoFisher Scientific) secondary antibodies, and immunoreactive proteins were visualized using enhanced chemiluminescence reagents (GE Healthcare). For immunoprecipitation, cells were lysed in lysis buffer containing 20 mM Tris [pH 7.5], 150 mM NaCl, 1% NP-40, 10% glycerol, and protease inhibitor mixture (Roche) for 1h. The lysed cells were clarified by centrifugation at 12,000 × g for 15 min. The supernatant was collected and protein

concentration was determined using a BCA protein assay kit (Thermo Scientific) according to the manufacturer's instructions. One milligram of protein was precleared in the presence of 20 μl Dynabead protein G (Thermo Scientific) for 1h at 4ºC. After centrifugation, the supernatant was collected and incubated with 1 μg of anti-caspase-8 antibody (Acris Antibodies, Herford, Germany) in the presence of 20 μL Dynabead protein G (Thermo Scientific). The precipitated beads were washed 3 times in lysis buffer and then the precipitated proteins were analyzed by Western blotting.

7. Caspase-8 activity analysis

Caspase-8 activity was measured using a Caspase-Glo 8 assay kit (Promega). OVCAR-3 or HeLa cells were treated with R27T (100 ng/mL), cFLIP siRNA (10 nM), and/or TBB (10 μM) alone or in combination, and then lysed on ice in phosphate buffered saline containing 1% NP40 and 0.1% SDS. Ten micrograms of cell lysate in a 50 μL total volume was resuspended in 50 μL of Caspase-Glo reagent and incubated for 1 h at room temperature. The luminescence produced upon cleavage of the luminogenic substrate (which contained the caspase-8 cleavage site, LETD) was measured for each sample using a microplate reader (TECAN).

8. Assessment of *in vivo* anti-tumor efficacy

The anti-tumor efficacy of R27T *in vivo* was tested in OVCAR-3 and HeLa xenograft models. All animal experiments were approved by the Institutional Animal Care and Use Committee (IACUC) of Seoul National University (SNU-160310-1). Five-week-old female athymic nude mice (Orient Bio, Seongnam, Gyeonggi, South Korea) were subcutaneously inoculated at the dorsal right side with 5 x 10^6 cells. OVCAR-3-tumor-bearing mice were intraperitoneally treated with R27T (1 mg/kg) every other day for three weeks. In HeLa xenograft model, the mice were intraperitoneally administered three times per week for 4 weeks with either vehicle or TBB (10 mg/kg) or/and R27T (1 mg/kg). In the co-treatment group, mice were treated with TBB and R27T alternately every day for 4 weeks. Tumor size was measured by caliper every other day in two dimensions, and the tumor volume was calculated using the following formula; tumor volume (mm^3) = (short diameter)^2 x (long diameter) x 0.5. For histological evaluation, tumor tissues were extracted, weighed, sectioned, and stained with TUNEL. In addition, expression level of cFLIP was determined by immunohistochemical staining HeLa tumor tissue section (4 μm thick) with an anti-cFLIP antibody (AG Scientific).

9. Statistics

Statistics were conducted by analysis of variance (ANOVA), with the Student-Newman-Keuls test. The SigmaStat software (Systat Software, Richmond, CA, USA) was employed, and $P < 0.05$ was considered statistically significant.

Results

1. R27T induces anti-proliferation and apoptosis

To investigate the anti-cancer efficacy of R27T *in vitro,* I carried out two different assays in OVCAR-3, MCF-7, HeLa, and TOV-21G cells. The cell proliferation assay revealed that R27T showed a concentration-dependent anti-proliferative effect in OVCAR-3 and MCF-7 cells, but not in HeLa or TOV-21G cells (Figure 1). Treatment of OVCAR-3 and MCF-7 cells with R27T decreased cell viability by 86.1 ± 2.1 and 60.4 ± 1.7% at 72 h post-treatment, respectively. In contrast, R27T did not significantly induce anti-cancer activity in HeLa cells compared with that in control cells. The live fluorescence assay system yielded similar results, which showed that R27T exerted notable cell-killing effects in OVCAR-3 and MCF-7 cells, but not in HeLa or TOV-21G cells (Figure 2).

Next, I examined whether R27T could induce apoptosis in OVCAR-3, MCF-7, HeLa, and/or TOV-21G cells. I found that the treatment of OVCAR-3 and MCF-7 cells with R27T increased the proportion of late-stage apoptotic cells to 78.3 and 40.0%, respectively, compared to less than 15% in the untreated cells. However, R27T treatment did not alter the population of late-stage apoptotic cells in HeLa or TOV-21G cells (Figure 3). Thus, the results suggest that R27T exhibits differential anti-proliferative and pro-apoptotic effects in R27T-sensitive cells (OVCAR-3 and MCF-7) versus R27T-resistant

cells (HeLa and TOV-21G).

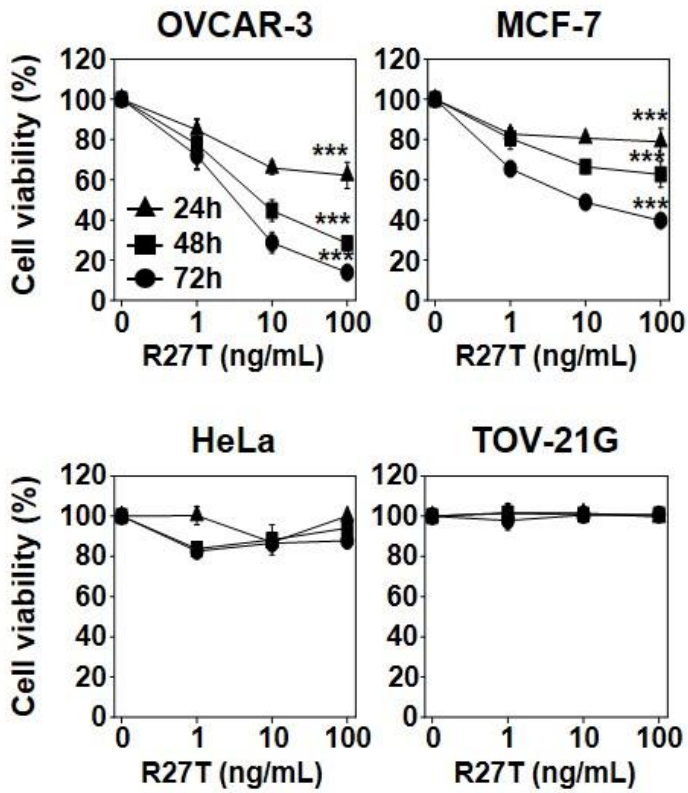

Figure 1. Analysis of anti-proliferative effects of R27T in different cell lines by WST assay. OVCAR-3, MCF-7, HeLa, or TOV-21G cells were treated with or without various concentrations of R27T. The cells were incubated for various times, and cell viability was measured by WTS assay. Data are presented as the mean ± SD of three independent experiments (***P < 0.001 compared to the untreated group).

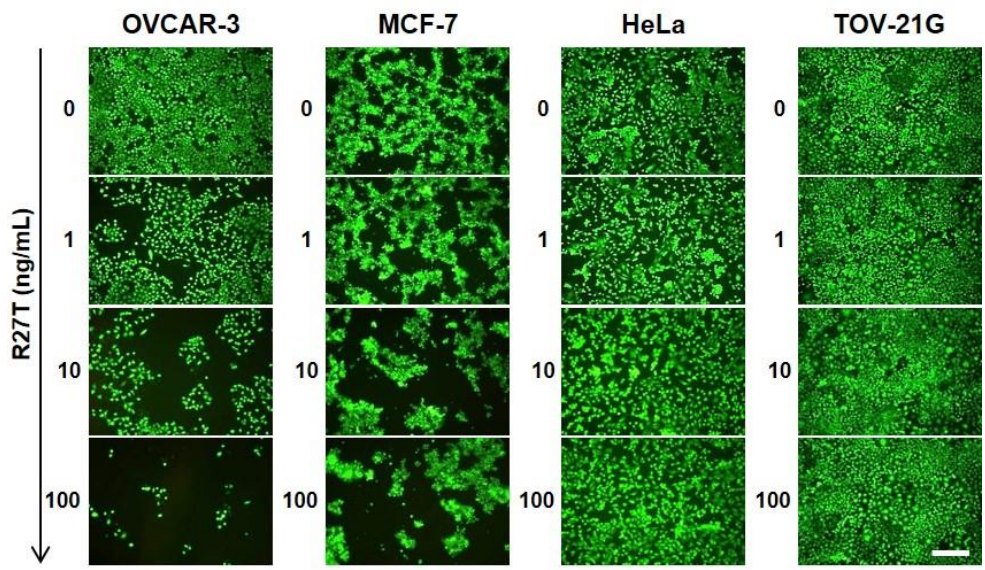

Figure 2. Analysis of anti-proliferative effects of R27T in different cell lines by live cell imaging. OVCAR-3, MCF-7, HeLa, or TOV-21G cells were treated with or without various concentrations of R27T. Seventy-two hours after treatment, live cells were incubated with calcein-AM and analyzed by microscopy for detection of fluorescence. Scale bar = 250 μm.

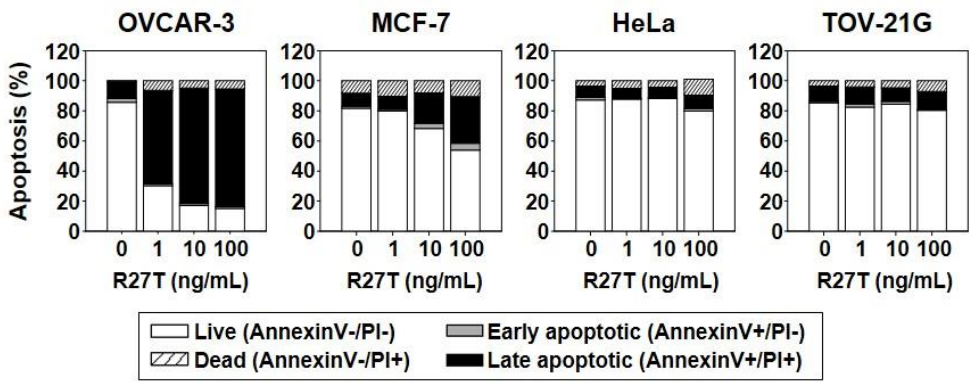

Figure 3. Pro-apoptotic effects of R27T in different cell lines. OVCAR-3, MCF-7, HeLa, or TOV-21G cells were treated with or without various concentrations of R27T. Apoptosis activity was quantified by bivariate flow cytometry of cells stained with Annexin V/PI at 72 h post-treatment.

2. Induction of apoptotic mediators does not correlate with R27T resistance

To investigate whether R27T resistance is related to IFN-induced signaling, I transiently transfected OVCAR-3 and HeLa cells with the interferon-sensitive response element (ISRE)-luciferase reporter plasmid. R27T treatment (100 ng/mL) resulted in 2.7- and 14.9-fold increase of ISRE luciferase activity in R27T-sensitive OVCAR-3 cells (Figure 4A) and R27T-resistant HeLa cells (Figure 4B), compared with their respective controls.

To examine whether R27T resistance was correlated with the induction of apoptotic mediators, I compared the mRNA and protein expression levels of DR4, FAS, TNF-α, and TRAIL in R27T-sensitive OVCAR-3 and R27T-resistant HeLa cells. qRT-PCR and western blotting analysis showed that the mRNA (Figure 5) and protein (Figure 6) expression levels of FAS, TNF-α, and TRAIL increased in both cell lines following R27T treatment. As shown by the results of western blot analysis, two sizes of FAS or TRAIL proteins were detected at 45/48 or 28/30 kDa, respectively (Figure 6). Previous reports showed that two molecular weights of FAS protein resulted from different glycosylation patterns [113], and TRAIL existed in two isoforms [114]. Overall, these results indicate that R27T resistance is not associated with changes in IFN-induced signal transduction or the induction of apoptotic mediators.

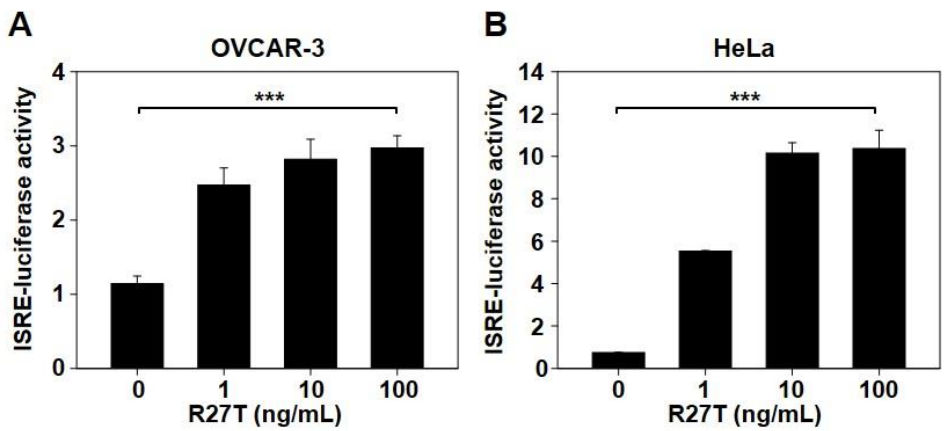

Figure 4. Ability of R27T to induce the IFN signaling. ISRE-luciferase-expressing OVCAR-3 (A) and HeLa cells (B) were treated with various concentrations of R27T for 16 h, and the ISRE luciferase activity was determined using a dual-luciferase kit.

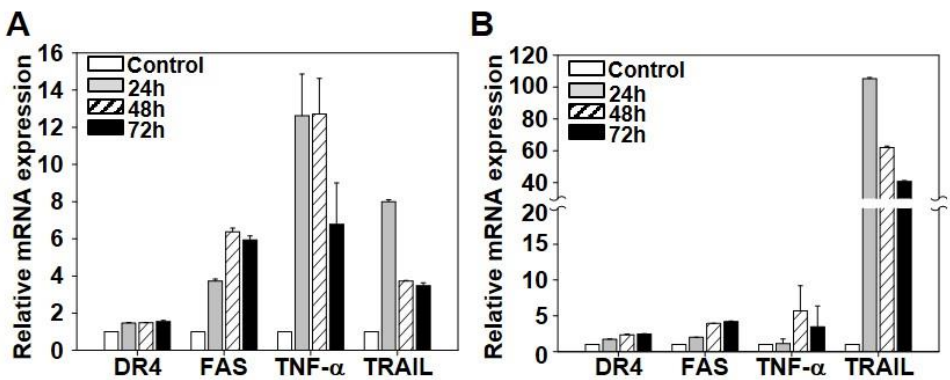

Figure 5. Ability of R27T to increase the mRNA expression of apoptotic mediators. OVCAR-3 (A) or HeLa cells (B) were treated with R27T (100 ng/mL) for the indicated times, and the mRNA levels were analyzed by qRT-PCR. Error bars indicate the SD of experiments performed in triplicate.

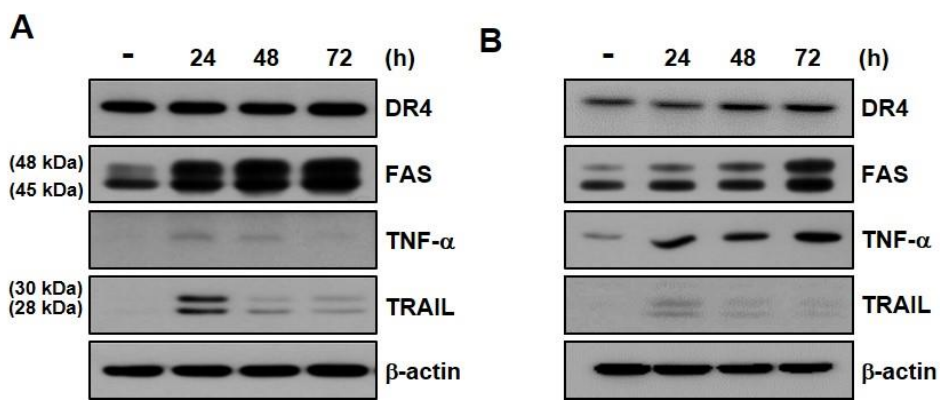

Figure 6. Ability of R27T to increase the ptorein expression of apoptotic mediators. OVCAR-3 (A) or HeLa cells (B) were treated with R27T (100 ng/mL) for the indicated times, and the mRNA and protein levels were analyzed by Western blot analysis, respectively. β-Actin was used as a loading control.

3. R27T-resistant cancer cells exhibit increased cFLIPS expression and blockade of caspase activation

To test whether changes in caspase activity contribute to R27T resistance, I examined caspase-8 activity in R27T-sensitive OVCAR-3 cells and R27T-resistant HeLa cells. Following R27T treatment, caspase-8 activity significantly and time-dependently increased up to 48 h post-treatment in OVCAR-3 cells (to 5.4-fold the basal activity; Figure 7A), but not in HeLa cells (Figure 7B). Western blotting analysis of caspase-8, -9, and -3 showed that these proteins were cleaved following R27T treatment of R27T-sensitive OVCAR-3 cells (Figure 8A) but not R27T-resistant HeLa cells (Figure 8B). These results demonstrated that the activation of caspase cascade might be blocked in R27T-resistant cells.

cFLIP is a crucial negative regulator of caspase-8 activation [115]. Therefore, I next examined the expression level of cFLIP in R27T-sensitive and -resistant cells. Increased expression of cFLIPL and cFLIPS was observed in HeLa cells compared to that in OVCAR-3 cells without R27T treatment. cFLIPS was not detected in OVCAR-3 cells (Figure 9). Notably, there was no difference in the expression level of cFLIP protein in OVCAR-3 cells after R27T treatment compared with that in the control cells (Figure 8A). In contrast, cFLIPS protein expression was significantly increased in R27T-treated HeLa cells at 72 h (Figure 8B). To substantiate these results, I sought to test whether the late increase of cFLIPS level is related to

transcription factors such as NF-κB and NFAT. I found that R27T treatment of both OVCAR-3 and HeLa cells did not significantly alter the NF-κB p65 levels for 72 h (Figure 10). However, the activation of p65 (phosphorylated p65) and NFAT1c (dephosphorylated NFAT1c) was greater in HeLa cells (Figure 10B) than in OVCAR-3 cells (Figure 10A). These results revealed that the late expression of cFLIPS in R27T-resistant cells might be influenced by the increased activation of p65 and NFAT1c following R27T treatment.

The co-treatment of OVCAR-3 cells with the pan-caspase inhibitor, zVAD, recovered cell viability by 89.1 ± 6.6% compared to less than 20% observed in OVCAR-3 cells treated with R27T alone (Figure 11). I ascertained whether the overexpression of cFLIPS plays a role in apoptosis resistance. When OVCAR-3 cells transfected with cFLIPS expression vector was treated with R27T, cell viability was restored to 81 ± 5.2% (Figure 12). Taken together, these results show that an increase in cFLIPS expression contributes to the impairment of caspase activation in R27T-resistant cells.

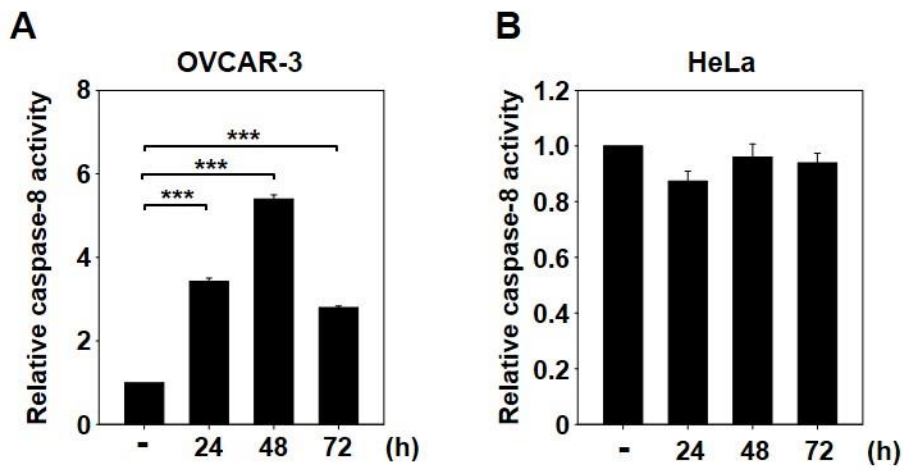

Figure 7. Ability of R27T to activate the caspase-8. Cells were treated with 100 ng/mL of R27T and collected at the indicated times post-treatment. Caspase-8 activity was assessed by protease activity assays in (A) OVCAR-3 or (B) HeLa cells (***$P < 0.001$ compared to untreated group).

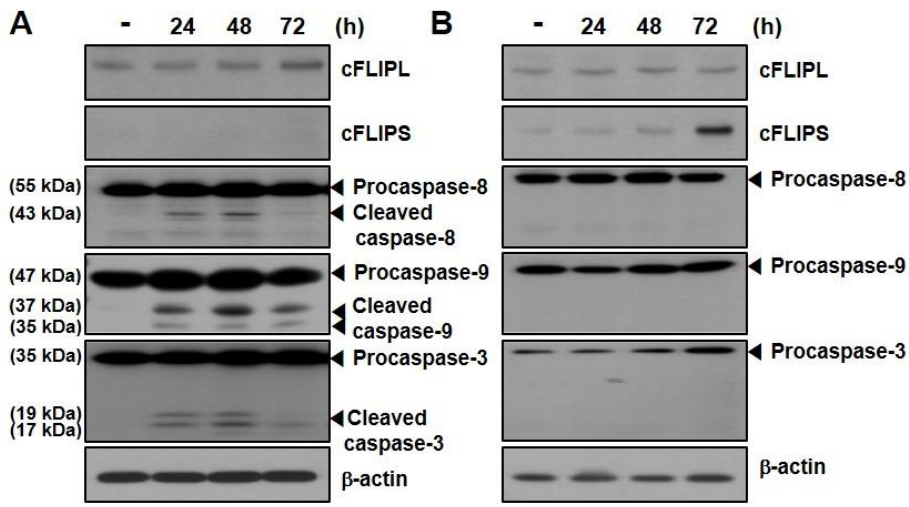

Figure 8. Ability of R27T to activate the caspase cascade and cFLIP expression. Cells were treated with 100 ng/mL of R27T and collected at the indicated times post-treatment. For detection of cleaved caspase-3/8, cFLIPL, and cFLIPS, Western blot analyses were performed in (A) OVCAR-3 or (B) HeLa cells. β-Actin was used as a loading control.

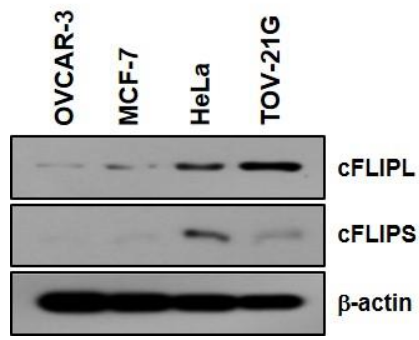

Figure 9. cFLIP expression in different cell lines. Protein expression of cFLIPL and cFLIPS was analyzed using western blotting in OVCAR-3, MCF-7, HeLa, or TOV-21G cells. β-actin was used as the loading control.

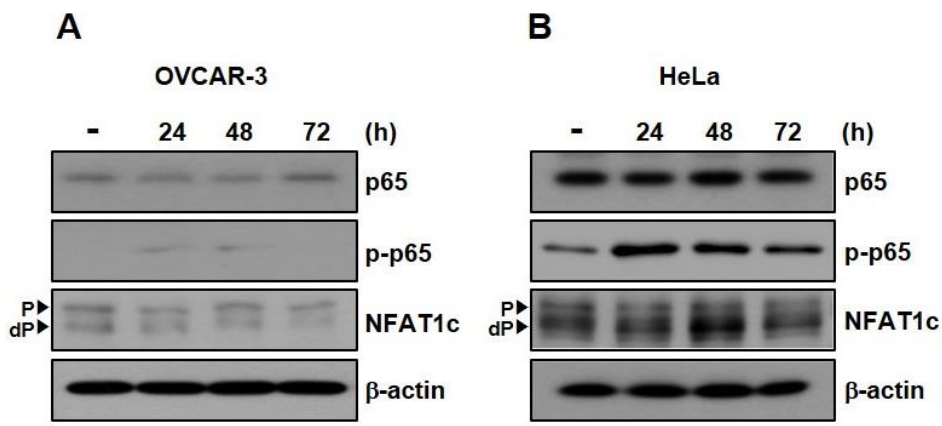

Figure 10. Activation of NF-κB p65 and NFAT1c by R27T treatment. OVCAR-3 (A) and HeLa (B) cells were treated with 100 ng/mL of R27T for the indicated time. For detection of p65, p-p65, and NFAT1c, western blot analysis was performed. β-actin was used as the loading control.

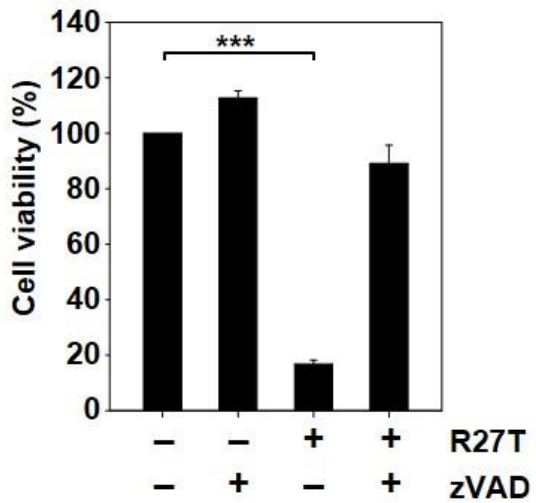

Figure 11. Inhibition of anti-proliferation efficacy of R27T by co-treatment with zVAD. OVCAR-3 cells were treated with R27T (100 ng/mL) alone or in combination with 50 μM zVAD for 72 h, and cell viability was measured by WTS assays. Data are presented as the mean ± SD of three independent experiments (***$P < 0.001$ compared to the untreated group).

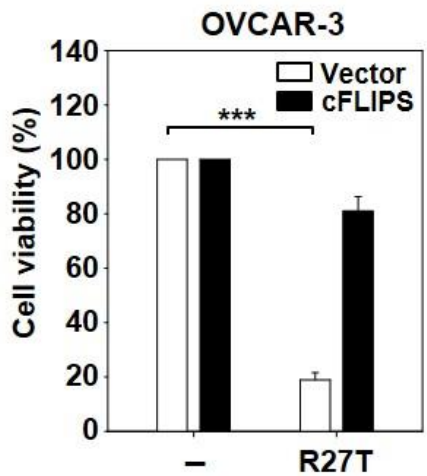

Figure 12. Inhibition of anti-proliferation efficacy of R27T by cFLIPS expression. OVCAR-3 cells transfected with control or cFLIPS vector were treated with 100 ng/mL R27T for 72 h. Cell viability was analyzed by WTS assays (***$P < 0.001$ compared to the untreated group).

4. Inhibition of cFLIP expression facilitates caspase activation

I further verified the effect of suppression of cFLIP on caspase-8 activity. Caspase-8 activity in HeLa cells treated with cFLIP siRNA plus R27T was 2.7-fold higher than that in HeLa cells treated with R27T alone (Figure 13A), and I detected the cleaved caspase-8 product (Figure 13B). A previous study reported that inhibition of CK-2 by TBB decreased the endogenous cFLIP levels via proteasome-mediated degradation of cFLIP, leading to the enhancement of TRAIL and FAS sensitivity in endometrial carcinoma cells [10]. Therefore, HeLa cells were co-treated with R27T and TBB, which resulted in the reduction of cFLIP expression. Furthermore, co-treatment of R27T with TBB resulted in 2.3-fold increase in caspase-8 activity (Figure 14A) and the cleavage of caspase-8 (Figure 14B). Immunoprecipitation of cFLIPL and cFLIPS with an anti-caspase-8 antibody revealed that TBB treatment did not inhibit cFLIP binding with caspase-8 but only decreased cFLIP expression, thereby activating caspase-8 on R27T co-treatment (Figure 15).

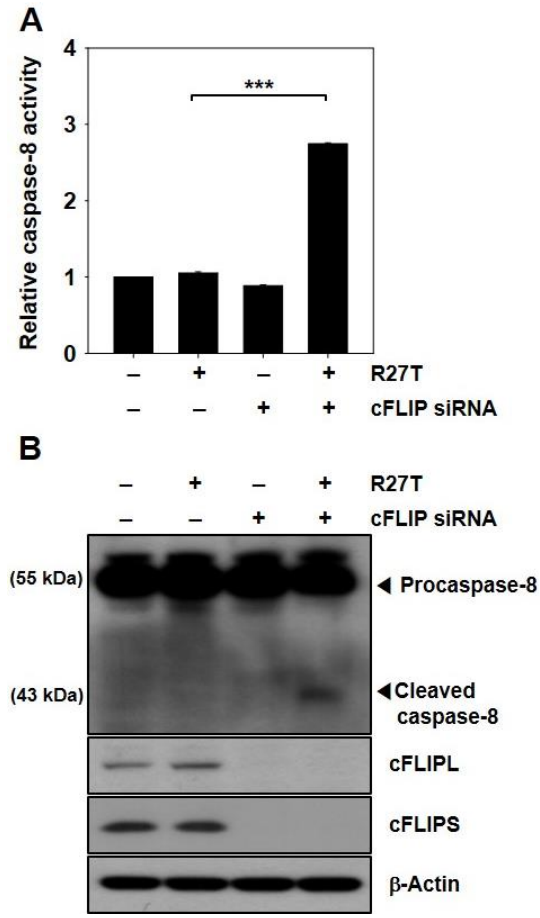

Figure 13. Inhibition of cFLIP expression with siRNA enhances caspase-8 activation in R27T-resistant cells. HeLa cells were transfected with 10 nM scrambled or cFLIP siRNA for 24 h, and then treated with R27T (100 ng/mL) for an additional 48 h. Cell lysates were analyzed by protease activity assays (A) or Western blot analyses (B). Data are presented as the mean ± SD of three independent experiments (***$P < 0.001$ compared to the untreated group). β-Actin was used as a loading control.

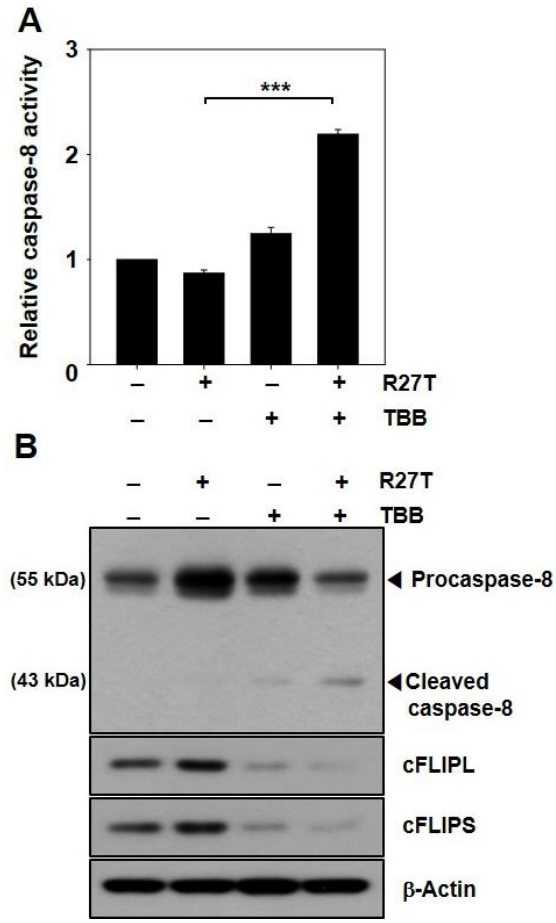

Figure 14. Inhibition of cFLIP expression with TBB enhances caspase-8 activation in R27T-resistant cells. HeLa cells were co-treated with 10 μM TBB in the absence or presence of R27T (100 ng/mL) for 48 h, and cell lysates were analyzed by protease activity assays (A) or Western blot analyses (B). Data are presented as the mean ± SD of three independent experiments (***P < 0.001 compared to the untreated group). β-Actin was used as a loading control.

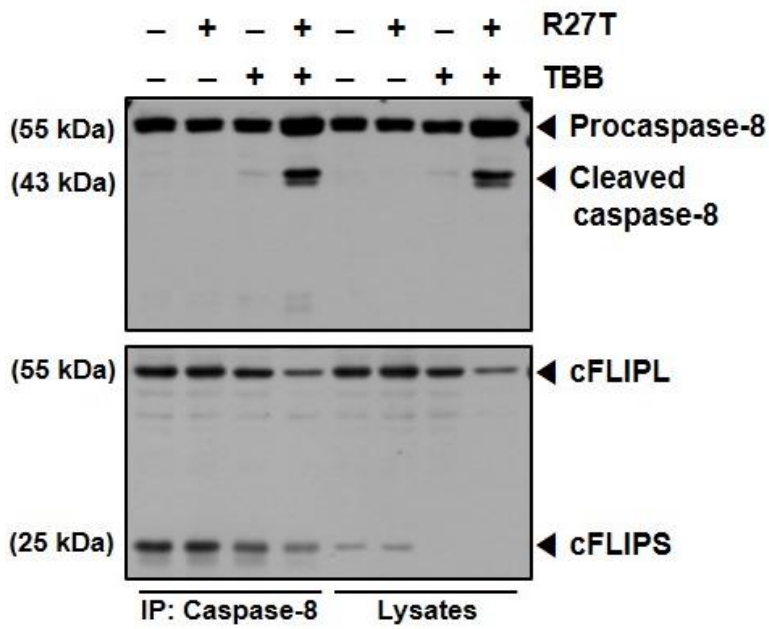

Figure 15. TBB-mediated reduction of cFLIP. HeLa cells were treated with 10 μM TBB in the absence or presence of R27T (100 ng/mL) for 48 h, and the cell lysates were used for western blotting before (lysates) or after (IP: Caspase-8) immunoprecipitation with an anti-caspase-8 antibody.

5. Inhibition of cFLIP expression sensitizes R27T-resistant cancer cells to anti-proliferative and pro-apoptotic effects

I next examined whether the cFLIP siRNA- or TBB-mediated inhibition of cFLIP expression could enhance the anti-cancer efficacy of R27T *in vitro*. In the WST assay system, combined treatment of R27T and cFLIP siRNA significantly reduced HeLa cell viability to 54.1 ± 2.5% (Figure 16A). For the establishment of cFLIP overexpression in HeLa cells, cFLIPL, cFLIPS, or cFLIPL + S vectors were transfected. Western blot assay showed an increase in cFLIP protein expression (Figure 18). The anti-cancer activity of R27T plus TBB was 2.1-, 3.0-, or 2.9-fold greater in control vector-transfected HeLa cells than in HeLa cells transfected with cFLIPL, cFLIPS, and cFLIPL + S vector, respectively (Figure 17A). In control vector-transfected HeLa cells, R27T plus TBB exerted 3.6-fold greater cell-killing effect compared with that of free R27T. Similarly, fluorescent microscopy revealed that the smallest live-cell populations were observed in cultures co-treated with R27T and cFLIP siRNA (Figure 16B) or TBB (Figure 17B). Moreover, apoptosis was significantly increased when HeLa cells were co-treated with R27T and cFLIP siRNA or TBB, with the late apoptotic cell populations increasing to 63.5 (Figure 16C) or 51.6% (Figure 17C) compared to less than 10% observed in the controls, respectively. These results suggest that the combined treatment of R27T and a cFLIP inhibitor can overcome R27T resistance and increase the therapeutic efficacy of R27T in resistant cells.

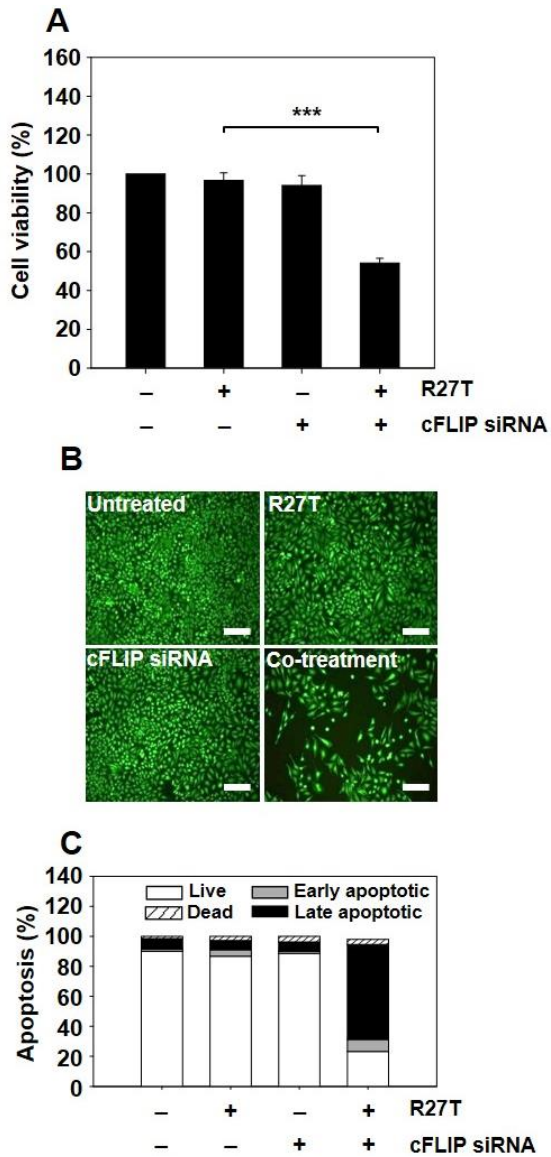

Figure 16. Inhibition of cFLIP expression with siRNA enhances R27T-induced anti-proliferation and apoptosis in R27T-resistant cells. HeLa

-continued next page-

cells were transfected with 10 nM of scrambled or cFLIP siRNA for 24 h, and then treated with R27T (100 ng/mL) for an additional 48 h. Cell viability was analyzed by WTS assays (A) or live-cell staining (B), and apoptosis was assessed by Annexin V/PI staining. Error bars indicate the SD of experiments performed in triplicate (***$P < 0.001$ compared to the R27T-treated group). Scale bar = 250 μm.

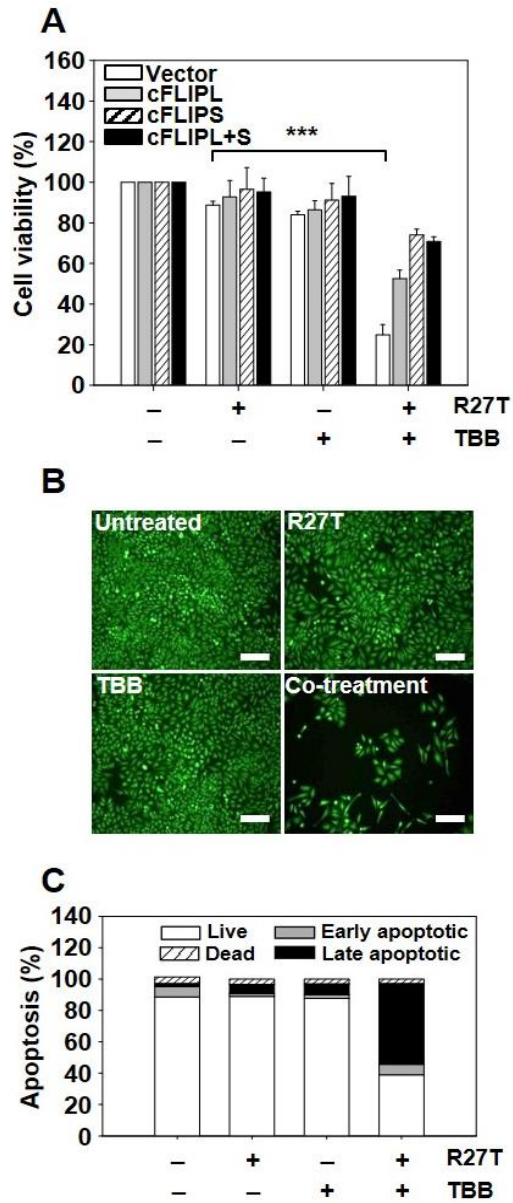

Figure 17. Inhibition of cFLIP expression with TBB enhances R27T-induced anti-proliferation and apoptosis in R27T-resistant cells. HeLa

-continued next page-

cells alone or transfected with cFLIPL, cFLIPS, or cFLIPL+S vector were treated with TBB (10 μM) and/or R27T (100 ng/mL) for 48 h. Cell viability was analyzed by WTS assays (A) and live-cell staining (B), while apoptosis was assessed by Annexin V/PI staining (C). Error bars indicate the SD of experiments performed in triplicate (***$P < 0.001$ compared to the R27T-treated group). Scale bar = 250 μm.

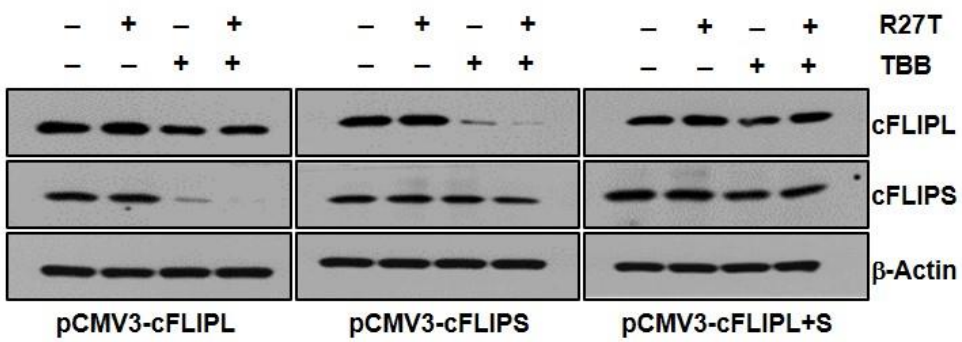

Figure 18. Restoration of cFLIP by expression vector transfection prior to TBB or R27T treatment. HeLa cells transfected with cFLIPL, cFLIPS, or cFLIPL + S vector were treated with TBB (10 mM) or R27T (100 ng/mL) or both for 48 h. For the detection of cFLIPL and cFLIPS, western blot analysis was performed. b-actin was used as the loading control.

6. Combined treatment with R27T and TBB suppresses *in vivo* tumor growth

I next examined the *in vivo* anti-tumor efficacy of R27T in an OVCAR-3 tumor xenograft model. The tumor volumes were significantly smaller (Figure 19A) and tumor weights were lower (Figure 19B and 19C) in mice treated with R27T than in those treated with the control vehicle. The tumor weight of R27T-treated group was 3.1-fold lower than that of the vehicle. When I further examined the anti-tumor effects of intraperitoneally co-administered R27T and TBB in HeLa tumor-bearing mice, significant inhibition of tumor growth was observed in the R27T/TBB co-treated group (Figure 20A). The tumor weights were lowest in the mice co-treated with R27T and TBB, which exhibited a 3-fold reduction in tumor weight compared with that of R27T-treated mice (Figure 20B and 20A). In keeping with these tumor-growth inhibition effects, terminal deoxynucleotidyl transferase dUTP nick end labeling (TUNEL) analysis showed population of apoptotic cells in OVCAR-3 tumor tissues of R27T-treated mice (Figure 19D) or HeLa tumor tissues of R27T plus TBB- treated mice (Figure 20D) was higher than that in the control-treated group. Furthermore, a significant decrease in cFLIP staining was observed in HeLa tumor tissues of R27T plus TBB-treated mice (Figure 21). Collectively, these results indicate that the anti-tumor activity of R27T could be enhanced by combination treatment with TBB.

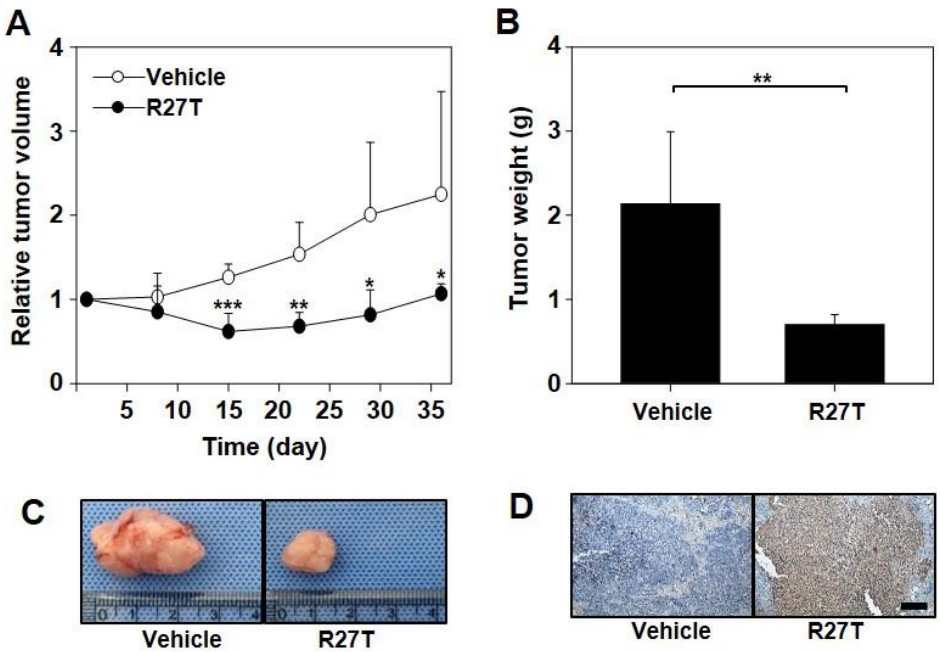

Figure 19. *In vivo* anti-tumor efficacy of R27T in OVCAR-3 xenograft mouse model. OVCAR-3-tumor-bearing mice were intraperitoneally treated with vehicle or R27T (1 mg/kg) three times per week for 3 weeks (n=5 per group). Tumor volumes were measured in each group (A). OVCAR-3 tumor tissues were extracted for weight analysis (B) and visualization (C) and, sectioned for TUNEL staning (D). **P* < 0.05 compared to other groups, as assessed by ANOVA and the Student-Newman-Keuls test. Scale bar = 100 μm.

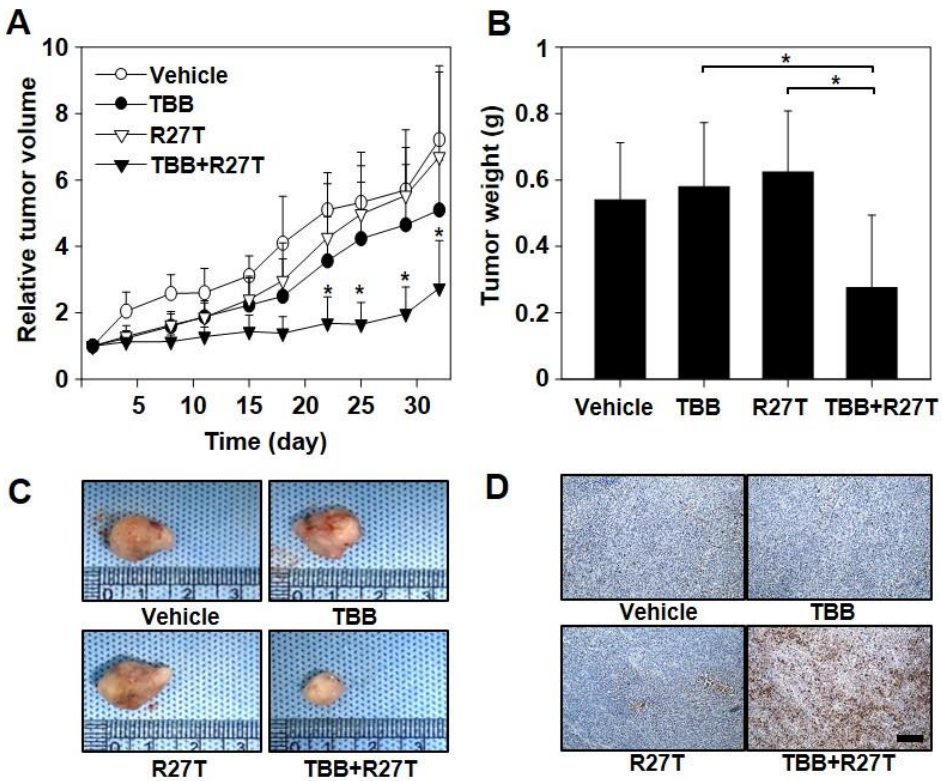

Figure 20. ***In vivo*** **anti-tumor efficacy of co-treatment with R27T plus TBB in HeLa xenograft mouse model.** HeLa-tumor-bearing mice were intraperitoneally treated three times per week for 4 weeks with either vehicle or TBB (10 mg/kg), and then with R27T (1 mg/kg; n=5 per group). Tumor volumes were periodically measured using calipers (A). HeLa tumor tissues were extracted for weight analysis (B) and visualization (C), and sectioned for TUNEL staning (D). *$P < 0.05$ compared to other groups, as assessed by ANOVA and the Student-Newman-Keuls test. Scale bar = 100 μm.

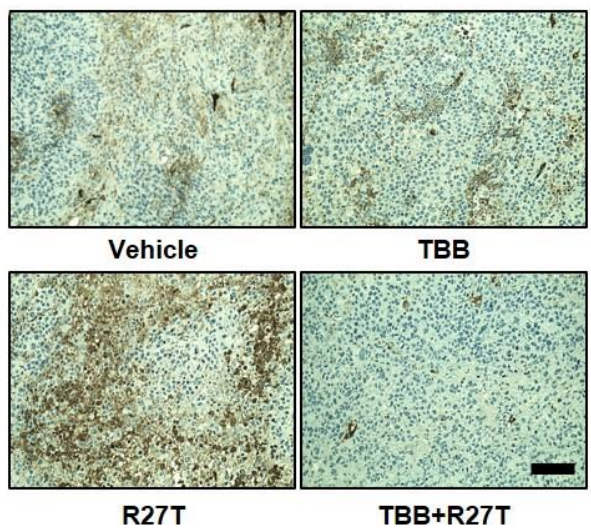

Figure 21. Immunohistochemical detection of cFLIP in HeLa tumor xenografts. HeLa tumor-bearing mice were intraperitoneally administered with TBB (10 mg/kg), R27T (1 mg/kg), or TBB + R27T (10 mg/kg TBB, 1 mg/kg R27T) three times per week for 4 weeks. Immunohistochemical staining of the tumor tissues was performed using anti-cFLIP antibody. Scale bar = 100 μm.

Discussion

In this study, I demonstrate the concentration-dependent anti-proliferative and pro-apoptotic effects of R27T in OVCAR-3 and MCF-7 cells via significant induction of IFN and death receptor signaling pathways. In contrast, R27T did not exhibit significant anti-cancer activity in HeLa cells, in which the overexpression of cFLIPS was associated with impaired caspase-8 activity and R27T resistance. Moreover, co-treatment with R27T and a cFLIP inhibitor was found to reduce the growth of R27T-resistant cells *in vitro* and *in vivo*.

It is notable that R27T has significant anti-cancer effects in OVCAR-3 and MCF-7 cells (Figure 1) because several previous reports have described the anti-proliferative effects of IFNβ in OVCAR-3 and MCF-7 cells [116, 117]. Consistent with our results, previous reports showed that IFNβ treatment did not induce apoptosis in HeLa cells [117, 118]. TOV-21G cells have a JAK1-truncating mutation [37], which suggests that R27T does not induce IFN signaling, enabling it to exert a dominant-negative effect on apoptosis (Figure 1C).

Unlike the nature of its anti-cancer effects, R27T increased ISRE luciferase activity and expression levels of apoptotic mediators in both OVCAR-3 and HeLa cells (Figure 4). It has been reported that IFN-stimulated gene factor-3 (ISGF-3) can bind to ISRE in OVCAR-3 or HeLa cells treated

with type I IFNs [119, 120]. Furthermore, the IFNβ-induced expression of interferon-stimulated genes (ISGs; e.g., DR4, FAS, TNF-α, and TRAIL) has been correlated with death receptor-mediated activation of apoptotic signals [3, 9, 121, 122]. Regardless of the activation of IFN and death receptor signaling pathways, there were significant differences in caspase activity between R27T-treated sensitive and -resistant cell lines (Figure 7 and 8). The caspase cascade can be initiated through either intrinsic (mitochondrial-mediated) or extrinsic (death receptor-mediated) apoptosis pathway. The extrinsic apoptosis pathway is triggered by ligand binding to death receptors, resulting in caspase-8 activation. Activated caspase-8 then directly cleaves effector caspases (caspase-3, -6, -7) or activates the intrinsic apoptotic pathway via cleavage of Bcl-2 homology (BH3)-interacting domain death agonist, resulting in caspase-9 activation. Activated caspase-9 then triggers apoptosis by activating effector caspases [123]. In this study, I found that the anti-cancer efficacy of R27T in OVCAR-3 cells was inhibited by the pan-caspase inhibitor, zVAD, which prevented R27T-mediated anti-proliferative effects (Figure 11), and has been used to study the mechanisms underlying the effects of IFNβ in various cancer cell lines [124, 125].

In the absence of R27T, cFLIPL and cFLIPS proteins were more highly expressed in R27T-resistant cells than in R27T-sensitive cells, thereby blocking caspase-8 activation (Figure 9 and Figure 8B). Moreover, when HeLa cells were treated with R27T for 72 h, an increase in cFLIPS expression

was observed (Figure 8B). cFLIP is known to be a major anti-apoptotic regulator and resistance factor that inhibits death receptor-induced apoptosis in a wide range of human malignancies [126, 127]. Recruitment of cFLIP to death-inducing signaling complex (DISC) prevents the processing and activation of procaspase-8 [126, 127]. Although 15 different isoforms of cFLIP have been currently identified, cFLIPL and cFLIPS are the major anti-apoptotic proteins [128, 129]. cFLIPL is structurally similar to procaspase-8 but lacks the catalytic cysteine residue and proteolytic activity, while cFLIPS only contains two N-terminal death effector domains [51]. In addition, cFLIPL forms heterodimeric complex with procaspase-8, resulting in the partial activation of caspase-8. Recruitment of cFLIPS to the DISC impedes homodimerization and activation of procaspase-8, preventing the downstream apoptosis cascade [54]. Notably, in an earlier report, TRAIL-induced upregulation of cFLIPS was shown to increase the survival of non-small cell lung carcinoma cells by reducing TRAIL sensitivity, whereas the cFLIPL isoform did not appear to be involved in TRAIL-induced apoptosis [130]. A previous report showed that cFLIPL triggered FAS-induced apoptosis upon strong receptor stimulation, while the overexpression of cFLIPS inhibited caspase-8 activation even upon expanded stimulation of FAS receptor [131]. Previous reports provided evidence that cFLIPS expression was significantly upregulated 72 h after TRAIL treatment [130], and cFLIPS expression was linked to the calcineurin/NFAT pathway in T-cells

[132]. NFAT can bind to cFLIP promoter, thereby promoting the expression of cFLIPS [132]. Activation of NF-κB enhanced histone deacetylase 1, reduced p300 and histone acetylation, and prevented the recruitment of NFAT to cFLIP promoter, resulting in the transcriptional repression of cFLIP [133]. The results of this study as well as previous studies suggest that R27T resistance of tumor cells might result from increased cFLIPS expression.

Downregulation of cFLIP by siRNA or TBB rendered R27T-resistant cells sensitive to R27T-mediated apoptosis and was accompanied by cleavage of caspase-8 (Figure 13-14 and Figure 16-17). Since the upregulation of cFLIP impairs caspase-8 activation, siRNA-mediated silencing of cFLIP could logically be predicted to promote the apoptosis of R27T-resistant cells. A previous report showed that the downregulation of cFLIP gene expression increased the pro-apoptotic effect of type I IFNs [134]. In addition, co-treatment with TRAIL and a cFLIP-targeting siRNA has been recently reported to enhance the apoptosis of TRAIL-resistant tumor cells via caspase-8 activation [135, 136]. Moreover, combined treatment with TRAIL and TBB was shown to increase the TRAIL sensitivity on cancer cells [137, 138]. Thus, I chose cFLIP siRNA and CK-2 inhibitor, TBB, for combination therapy with R27T.

In conclusion, this study is the first to show that the induction of apoptosis in cancer cells by R27T involves a cFLIP-mediated mechanism. I further suggest that it may be possible to enhance the therapeutic efficacy of

R27T significantly by downregulating cFLIP. Thus, combination therapy with R27T and cFLIP inhibitors may be an attractive strategy for overcoming R27T resistance.

PART II

The development anti-ERBB-2 antibody-glycoengineered interferon-β1a mutein fusion protein for gastric cancer therapy

Introduction

Gastric cancer is an aggressive disease that constitutes the second leading cause of cancer death worldwide [139]. Although fluoropyrimidine (anti-metabolite)- or platinum-based combination chemotherapies are widely accepted for advanced gastric cancer, their benefits have not necessarily translated to higher overall survival rates [140, 141]. Therefore, more effective therapies for gastric cancer are required.

The human epidermal growth factor receptor (HER) family is composed of EGFR, ERBB-2, ERBB-3, and ERBB-4 [142]. These molecules affect cell proliferation, differentiation, and apoptosis through homodimerization- or heterodimerization-mediated signaling [143]. In tumors, the overexpression of HER family members is often related to malignancy [144]. In gastric cancer, overexpression of EGFR, ERBB-2, and ERBB-3 has been reported and related to a less favorable prognosis [145]. Thus, inhibition of ERBB-2 signal transduction might benefit for patients with gastric cancer. In 2010, a ToGA (Trastuzumab for Gastric Cancer) trial showed that the combination of trastuzumab (human anti-ERBB-2 monoclonal antibody) and chemotherapy exhibited a survival benefit in ERBB-2-overexpressing gastric cancer patients [146]. At present, trastuzumab is FDA approved for the combined treatment with cisplatin and a fluoropyrimidine for ERBB-2-positive (ERBB-2+) metastatic gastric and gastroesophageal junction cancer.

The potential benefit of therapeutically enhancing the immune response against tumors has been discussed for the past few decades [147]. Clinical trials have examined the therapeutic efficacy of several cytokines in cancer patients [148], but it is difficult to administer therapeutically effective doses of such agents due to their considerable side effects and insufficient pharmacokinetic properties [149]. Recently, recombinant protein technology has allowed the construction of antibody-cytokine fusion proteins (also known as immunocytokines), which utilize the tumor-targeting ability of monoclonal antibodies to carry cytokines specifically to tumor sites where they might stimulate an enhanced anti-tumor immune response while decreasing systemic toxicity [76, 78, 150]. Among the diverse cytokines, type I IFNs has the great advantages of: clinical experience [151]; stimulation of T-cell immunity [152], the maturation of antigen presenting cells [153], enhancement of antibody-dependent cellular cytotoxicity (ADCC) [154], and direct tumor cell killing effect [155]; and inhibition of angiogenesis [156] (Table 1). IFN therapy has been reported to increase the anti-cancer immune response of ERBB-2-targeting therapeutics, such as trastuzumab and lapatinib [21, 44]. Therefore, combining anti-ERBB2 therapy with IFN could potentially benefit ERBB-2+ cancer patients.

In this study, I generated a trastuzumab-R27T fusion protein and examined its ability to specifically target ERBB-2+ gastric cancer cells. Our results show that R27T-fused trastuzumab exhibits higher expression level in

CHO-S cells compared to wild type IFNβ-fused trastuzumab. Moreover, the fusion protein properly induced IFN signaling and direct cell death in gastric cancer cells. Also, I have verified the antibody-dependent cellular cytotoxicity (ADCC) and complement dependent cytotoxicity (CDC) using fusion protein in gastric cancer cells and compared those efficacies with trastuzumab.

Table 1. Properties of cytokines under evaluation for cancer immunotherapy

Cytokine	Anti-tumor effect	ADCC enhancement	APC activation	T cell stimulation	Angiogenesis inhibition	Clinical experience
IL-2	-	+	-	+	-	+
IL-7	-	-	-	+	-	-
IL-12	-	+	-	+	+/-	+/-
IL-15	-	+	-	+	-	-
IL-18	-	+	-	+	+/-	-
IL-21	+/-	+	-	+	-	+/-
GM-CSF	-	+	+	+	-	+
IFNα/β	+	+	+	+	+	+

Materials and methods

1. Preparation of Trastuzumab and Trastuzumab-R27T

The trastuzumab and trastuzumab-R27T-expressing genes were prepared by gene synthesis (Cosmogenetech, Seoul, Korea), and the synthesized heavy and light chain DNAs were inserted into the pCHO 1.0 expression vector (Life Technologies, Gaithersburg, MD, USA) at the AvrII-Bstz17I and EcoRV-PacI sites of the polylinker region, respectively. CHO-S cells (Life Technologies) were transfected with the expression vectors, and stable clones were selected with 100-1000 nM of methotrexate (Sigma Aldrich) and 10-50 μg/mL of puromycin (Life Technologies). Culture fluids from CHO-S cells stably expressing trastuzumab and trastuzumab-R27T were collected and loaded onto a MabSelect SuRe™ rProtein A agarose-based resin (GE Healthcare), and the proteins were eluted using 0.1 M sodium citrate (pH 3.0) buffer.

2. Cell lines and culture condition

The NCI-N87 human gastric carcinoma cell line and normal primary human umbilical vein endothelial cells (HUVECs) were purchased from the American Type Culture Collection (ATCC; Manassas, VA, USA). The NCI-N87 cells were cultured in RPMI-1640 (HyClone, Logan, UT, USA) supplemented with 10% fetal bovine serum (HyClone), 100 units/mL

penicillin, and 100 μg/mL streptomycin (HyClone). HUVECs were maintained in VascuLife EnGS (containing Endothelial Cell Growth Supplement; Lifeline Cell Technology, Frederick, MD, USA). All cells were grown at 37ºC in a humidified 5% CO2 atmosphere.

3. Cell viability assay

The *in vitro* anti-proliferation efficacy of R27T was tested using viability assays. NCI-N87 cells and HUVECs were seeded to 96-well plates, cultured overnight, and treated with or without various concentration of R27T, trastuzumab, or trastuzumab-R27T for 72 h. Cell viability was assessed using a water-soluble tetrazolium (WST) colorimetric assay (Ez-Cytox; Daeil Lab Service, Seoul, Korea). Briefly, 10 μl of WST reagent was added to each well, the plates were incubated for 1 h, and absorbance was measured at 430 nm using a microplate reader (TECAN, Männedorf, Switzerland).

4. Luciferase reporter assay

Reporter gene assays were performed using iLITE Type 1 IFN assay ready cells (Euro Diagnostica, Malmo, Sweden) and a Luciferase Assay kit (Promega, Madison, WI, USA). Briefly, iLITE Type 1 IFN assay ready cells were seeded to 96-well plates and treated with the indicated concentrations of R27T, trastuzumab, or trastuzumab-R27T. After 18 h, the activities of firefly luciferase were determined using a microplate reader (TECAN).

5. Antibodies and western blot analysis

NCI-N87 cells were treated with R27T (100 ng/mL), trastuzumab (100 ng/mL), or trastuzumab-R27T (100-300 ng/mL), and lysed in RIPA lysis buffer (150 mM sodium chloride, 1% Triton X-100, 1% sodium deoxycholate, 0.1% SDS, 50 mM Tris-HCl [pH 7.5], 2 mM EDTA) supplemented with a protease inhibitor mixture (Roche, Indianapolis, IN, USA). The lysed cells were incubated for 20 min on ice and clarified by centrifugation at 12,000 × g for 15 min. The supernatant was collected and the protein concentrations were determined using a BCA protein assay kit (Thermo Scientific, Pittsburgh, PA, USA) according to the manufacturer's instructions. Twenty micrograms of protein were resolved by 12% SDS-PAGE and transferred to a polyvinyl difluoride membrane (PVDF; BioRad, Hercules, CA, USA). The PVDF membranes were blocked in TBS-Tween20 buffer containing 5% skim milk and incubated with primary antibodies at 4°C overnight. The utilized primary antibodies were anti-pSTAT1 (Cell Signaling Technology, Danvers, MA, USA) and anti-β-actin (Santa Cruz Biotechnology, Santa Cruz, CA, USA). The blots were then incubated for 1 h with anti-mouse IgG-HRP (ThermoFisher Scientific, San Jose, CA, USA) or anti-rabbit IgG-HRP (ThermoFisher Scientific) secondary antibodies, and immunoreactive proteins were visualized using enhanced chemiluminescence reagents (Amersham Biosciences, Piscataway, NJ, USA).

Culture fluids (10 μl) from CHO-S cells transiently expressing

trastuzumab-IFNβ-1a or trastuzumab-R27T were subjected to 12% SDS-PAGE, and the resolved proteins were transferred to a PVDF membrane (BioRad). The PVDF membranes were blocked in TBS-Tween20 buffer containing 5% skim milk and incubated with anti-human IgG-HRP (GenScript, Piscataway, NJ, USA). Immunoreactive proteins were visualized using enhanced chemiluminescence reagents (Amersham Biosciences).

6. Coomassie blue staining

The purified R27T, trastuzumab, or trastuzumab-R27T proteins were mixed with 5x protein sample buffer; reducing samples were mixed with DTT-supplemented 5x protein sample buffer and boiled, while non-reducing samples were mixed with DTT-free 5x protein sample buffer without boiling. The prepared samples were resolved by 12% SDS-PAGE and stained with coomassie blue staining solution.

7. Antibody-dependent cell-mediated cytotoxicity (ADCC) and complement-dependent cytolysis (CDC) assays

NCI-N87 cells and HUVECs were seeded to 96-well plates (target cells, 2x104 cells/well) and cultured overnight. For the ADCC assay, NK-92MI-CD16 cells were used as effector cells; the target cells were incubated for 6 h in the presence of trastuzumab or trastuzumab-R27T (final concentration: ~ 10 μg/mL) and 8x104 NK-92MI-CD16 cells (effector/target [E/T] ratio: 8).

For the CDC assay, human serum (Sigma Aldrich) was used as a complement source; the target cells were incubated with trastuzumab or trastuzumab-R27T (final concentration: ~ 10 μg/mL) and 20% human serum (v/v) for 6 h, and target cell viability was analyzed with the WST assay.

8. Flow cytometry analysis

The expressions of HER2 on the surfaces of NCI-N87 cells and HUVECs were evaluated using flow cytometric analysis. Cells were harvested, blocked for 1 h at 4°C in cold phosphate-buffered saline (PBS) containing 2% fetal bovine serum (HyClone). The cells were then washed twice with PBS, incubated for 1 h at 4°C with 1 μg of trastuzumab or trastuzumab-R27T (diluted in cold PBS), and then incubated with fluorescein isothiocyanate (FITC)-conjugated anti-human secondary antibody (diluted 1:100; Santa Cruz Biotechnology). HER2-expressing cells were identified by detection of monoclonal fluorescent antibodies using a BD FACSCalibur system equipped with the Cell Quest Pro software (BD Biosciences, San Jose, CA, USA).

9. Confocal microscopy analysis

NCI-N87 cells and HUVECs were seeded to 4-well culture slides (SPL, Seoul, Korea), cultured overnight, fixed with 4% paraformaldehyde in PBS for 15 min, and stained with trastuzumab or trastuzumab-R27T for 1 h. The cells were rinsed twice with PBS, incubated with FITC-conjugated anti-

human secondary antibody (Santa Cruz), and stainedwith 4,6-diamidino-2-phenylindole dihydrochloride (DAPI). The 4-well culture slides were removed from the chamber and mounted for digital micrographs, which were taken using a LSM 700 ZEISS laser scanning confocal microscope (Carl Zeiss, Jena, Germany). The data were processed using the LSM Colocalization Software (Carl Zeiss).

10. Three-dimensional structure, circular dichroism (CD) and size study

The three-dimensional structure of tratuzumab-R27T was predicted using the PDB data files for trastuzumab and IFNβ-1a. To determine the secondary structures of trastuzumab-R27T, CD spectra were obtained using a Chirascan-plus circular dichroism spectrometer (Applied Photophysics Ltd., Surrey, United Kingdom). The spectra were measured between the wavelengths of 190 and 260 nm in the presence of PBS. The secondary structure content of the trastuzumab-R27T was analyzed using the CDNN secondary structure analysis software (Applied Photophysics Ltd.). The size of trastuzumab-R27T was measured using dynamic light scattering.

11. Statistics

Statistical analyses were performed using analysis of variance (ANOVA) with the Student–Newman–Keuls test employed as a post hoc test. SigmaStat software (version 3.5, Systat Software, Richmond, CA, USA) was used for the analyses and a $P < 0.05$ was considered statistically significant.

Results

1. Design of Trastuzumab-R27T fusion protein

I generated an anti-ERBB2 antibody (trastuzumab)-R27T fusion protein (Figure 1) in which a 15-mer flexible peptide linker (GGGGSGGGGSGGGSG) was used to link R27T to the C-terminus of the heavy chain of trastuzumab. Therefore, a trastuzumab-R27T fusion protein has 2 R27T and the molar equivalent with R27T is 3.76. The recombinant DNA technology was used to fuse tastuzumab and R27T, the nucleotide sequence of trastuzumab, flexible linker and, R27T were prepared using gene synthesis.

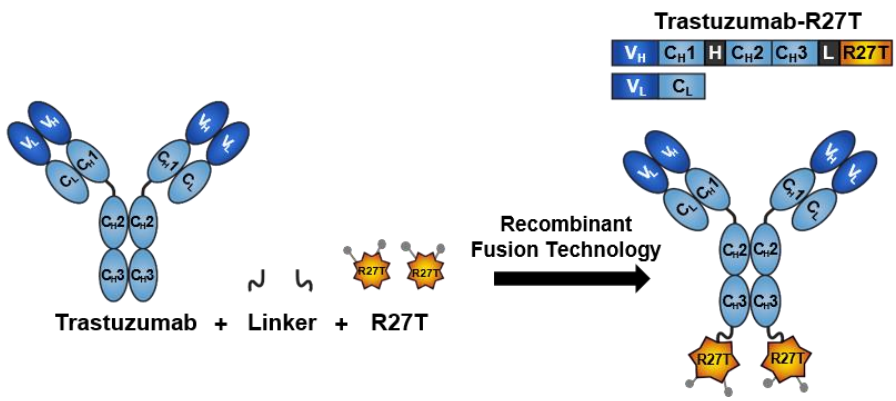

Figure 1. Schematics of trastuzumab-R27T and its constituents. The trastuzumab-R27T fusion protein was generated by fusing R27T to the C-terminus of the trastuzumab heavy chain via 15-mer flexible peptide linker (GGGGSGGGGSGGGSG). Abbreviations: V, variable (blue); C, constant (light blue); H, hinge; and L, linker.

2. Expression analysis of the trastuzumab-R27T fusion protein

R27T, trastuzumab, or trastuzumab-R27T were expressed in CHO cells and secreted to the culture medium. The proteins were purified and separated by SDS-PAGE under reducing (Figure 2A) and non-reducing (Figure 2B) conditions. The known molecular masses of trastuzumab and R27T are 146 kDa and 26 kDa, respectively [107, 157]. The band representing the heavy chain of the fusion protein was observed between the 70- and 100-kDa marker bands, confirming that R27T was successfully fused to the heavy chain (Figure 2A). The fusion protein showed a higher molecular mass compared to the trastuzumab band under non-reducing conditions (Figure 2B). Next, I compared the expression levels of trastuzumab-wild-type IFNβ-1a and trastuzumab-R27T fusion proteins in CHO-S cells. Expression vectors encoding trastuzumab-IFNβ-1a or trastuzumab-R27T were transfected into CHO-S cells, the cells were incubated for 48 h, and Western blotting was performed with anti-Human-IgG (H+L) antibody. Our analysis revealed that R27T-fused trastuzumab was expressed at a higher level than IFNβ-1a-fused trastuzumab (Figure 3A). Indeed, our IgG quantification analysis revealed that the expression level of trastuzumab-R27T was 6-fold higher than that of trastuzumab-IFNβ-1a (Figure 3B). Altogether these results suggest that trastuzumab-R27T is stably fused. Moreover, since the expression level is a critical factor in protein drug development, our results suggest that trastuzumab-R27T could be more therapeutically potent than trastuzumab-IFNβ-1a.

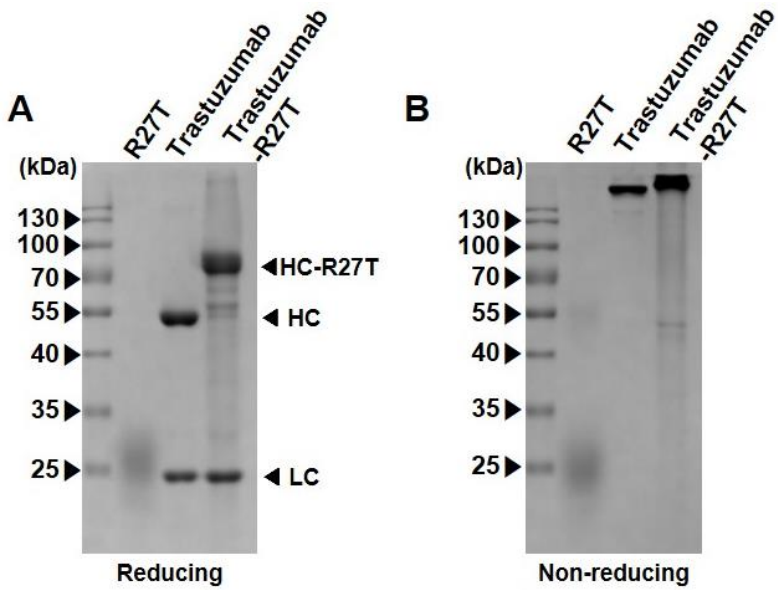

Figure 2. Purification of trastuzumab-R27T. CHODG44 cells were stably transfected with the R27T expression vector, while CHO-S cells were stably transfected with expression vectors encoding trastuzumab or trastuzumab-R27T. Proteins were purified from culture fluids using Sepharose 6FF columns (R27T) or Protein A columns (trastuzumab and trastuzumab-R27T) and separated by SDS-PAGE under (A) reducing conditions and (B) non-reducing conditions.

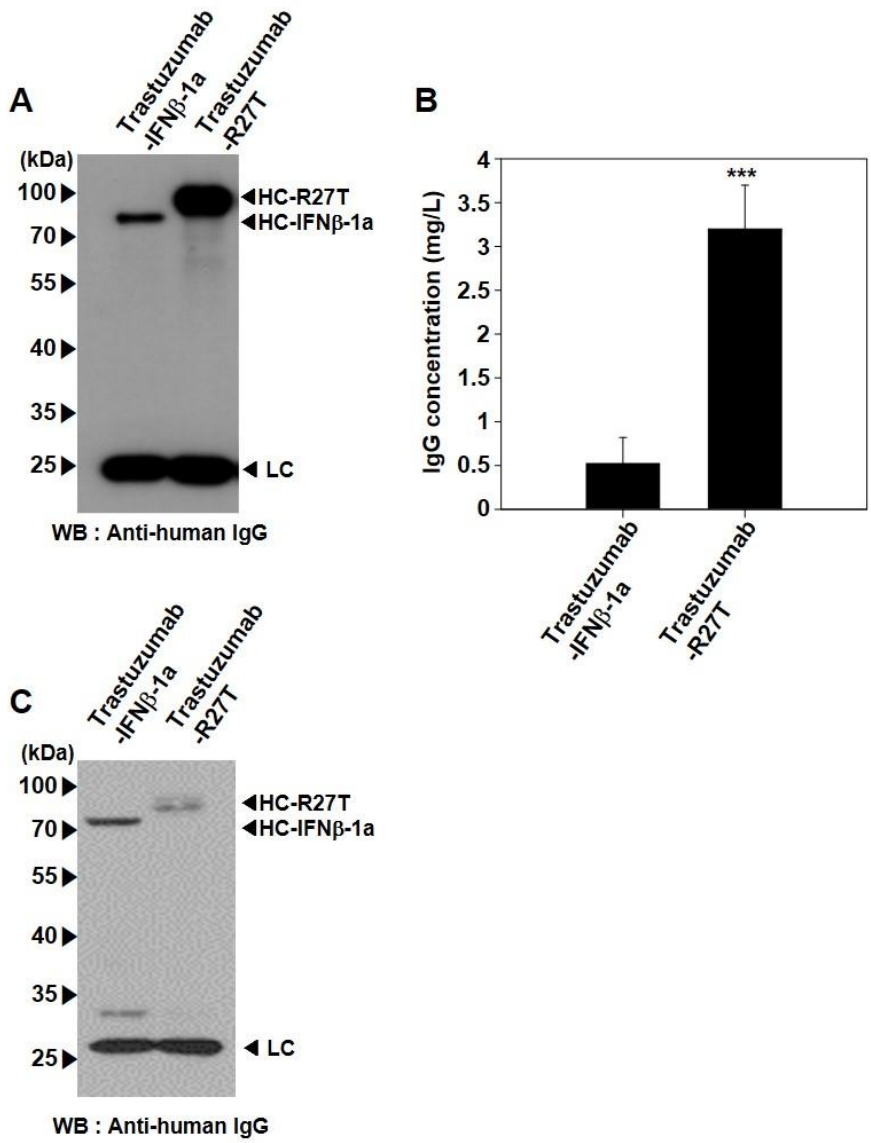

Figure 3. Comparison of expression level between trastuzumab-IFNβ-1a and trastuzumab-R27T. CHO-S cells were transfected with expression

-continued next page-

vectors encoding trastuzumab-IFNβ-1a or transtuzumab-R27T and incubated for 48 h, and culture fluids (A) or lysate (C) were subjected to Western blot analysis with anti-human IgG (H+L) antibody to detect the heavy and light chains, or (B) analyzed using a Cedex bio IgG quantification system. Data are presented as the mean ± SD of three independent experiments (***$P < 0.001$ between two groups).

3. Three-dimensional structure, size, and secondary structure analysis of trastuzumab-R27T

The three-dimensional structure of trastuzumab-R27T was visualized using the PDB data files for trastuzumab and IFNβ-1a (Figure 4A). The size of trastuzumab-R27T was 16.8 nm (Figure 4B) when analyzed by using dynamic light scattering. Furthermore, I observed a CD peak of trastuzumab-R27T at a zero intensity of 206 nm, and identified a spectral minimum at 220 nm (Figure 5C).

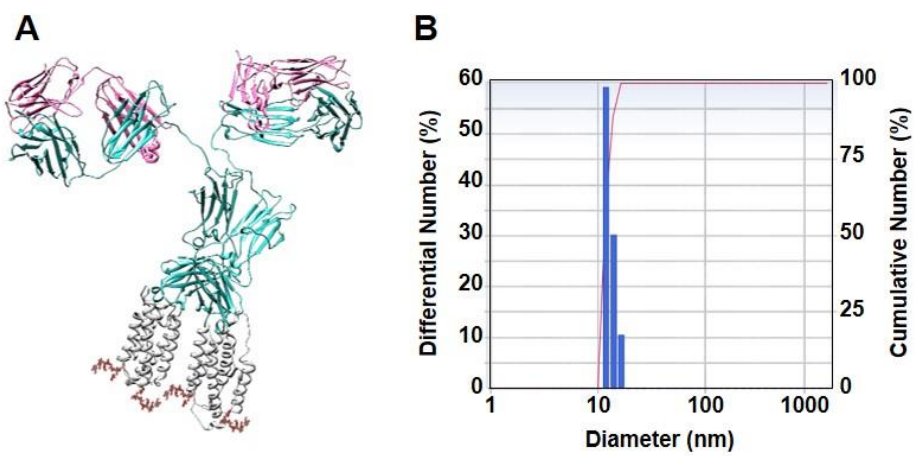

Figure 4. Size analysis of trastuzumab-R27T. (A) The three-dimensional structure of trastuzumab-R27T was predicted *in silico*. (B) The size of trastuzumab-R27T was measured by dynamic light scattering.

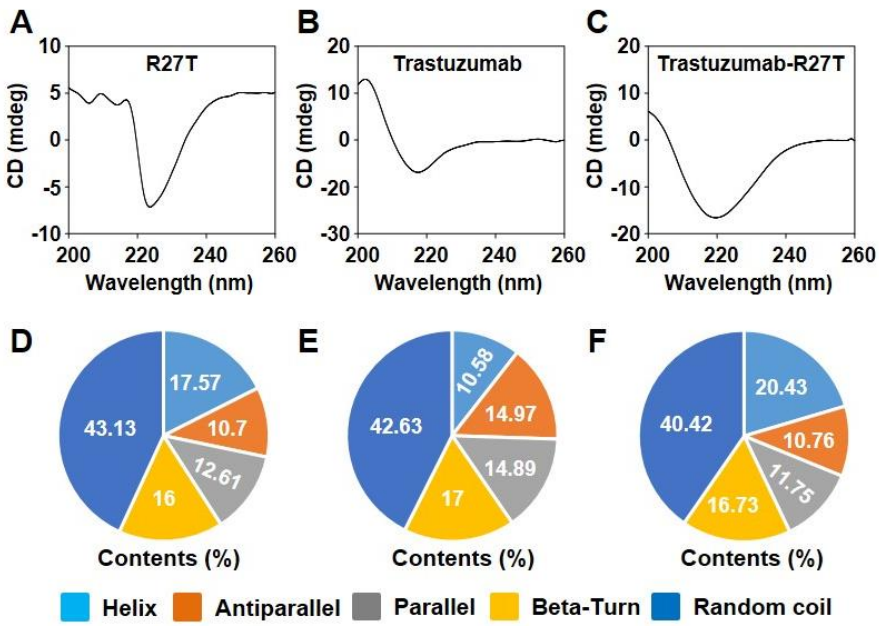

Figure 5. Structural analysis of trastuzumab-R27T. The CD spectra of (A) R27T, (B) trastuzumab, and (C) trastuzumab-R27T were measured. The secondary structural contents of (D) R27T, (E) trastuzumab, and (F) trastuzumab-R27T were analyzed using the CDNN program.

4. IFN bioactivity of trastuzumab-R27T

To investigate whether the bioactivity of IFN was maintained in the trastuzumab-R27T fusion protein, I applied an IFN assay system that utilizes U937 cells expressing firefly luciferase under the control of an IFN-responsive promoter. I found that trastuzumab-R27T dose-dependently increased luciferase activity in this system. Similar luciferase activities were observed in cells treated with 100 ng/mL R27T and 200 ng/mL trastuzumab-R27T (Figure 6A). IFNβ activity is mediated through the binding of type I IFN receptors and the subsequent phosphorylation of STATs [158]. In this study, I found that trastuzumab-R27T induced robust phosphorylation of STAT1 in NCI-N87 gastric cancer cells (Figure 6B). Overall, these results indicate that R27T is functional when fused to trastuzumab.

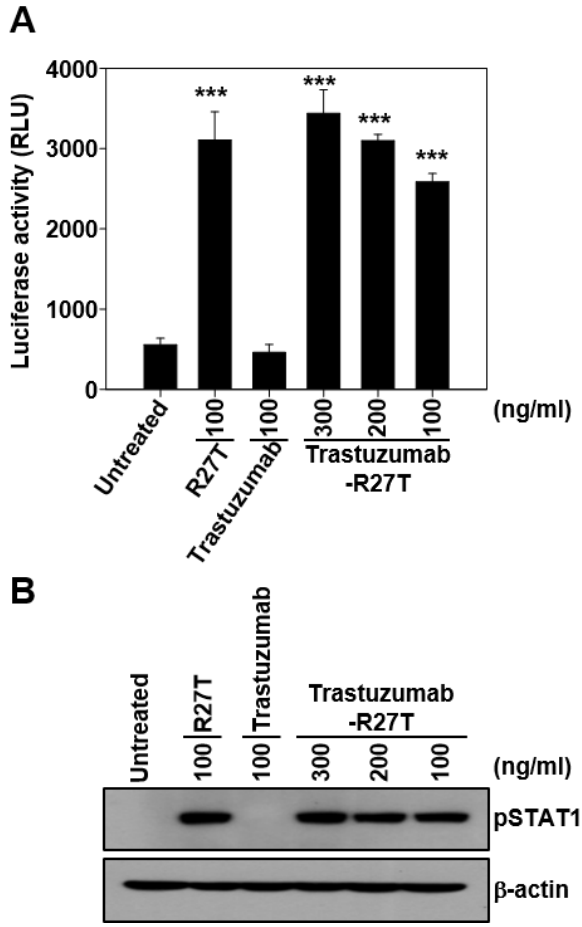

Figure 6. IFN functions of trastuzumab-R27T. (A) U937 cells stably expressing an ISG promoter-firefly luciferase gene were treated with or without the indicated concentrations of R27T, trastuzumab, or trastuzumab-R27T. After 18 h, the firefly luciferase activities were determined. (B) NCI-N87 cells were treated with or without various concentrations of R27T, trastuzumab, or trastuzumab-R27T for 1 h, and cell lysates were analyzed by

-continued next page-

Western blotting with indicated antibodies. Data are presented as the mean ± SD of three independent experiments (***$P < 0.001$ compared to the untreated group). β-actin was used as a loading control.these results show that the ERBB-2 targeting ability of R27T-fused trastuzumab is equivalent to that of trastuzumab.

5. Targeting of ERBB-2 by trastuzumab-R27T

To determine whether trastuzumab-R27T maintained the ERBB-2-targeting function, I stained ERBB-2-negative (ERBB-2-) HUVECs or ERBB-2+ NCI-N87 cells with trastuzumab or the fusion protein and performed FACS (Figure 7) and confocal microscopy (Figure 8). The FACS analysis revealed that trastuzumab and the fusion protein showed similar fluorescence intensities in both cell lines (Figure 7), indicating that the fusion protein retained the ability to target ERBB-2. Furthermore, confocal microscopy analysis revealed that the NCI-N87 cell membrane stained positively by the fusion protein (Figure 8B). Together, these results show that the ERBB-2 targeting ability of R27T-fused trastuzumab is equivalent to that of trastuzumab.

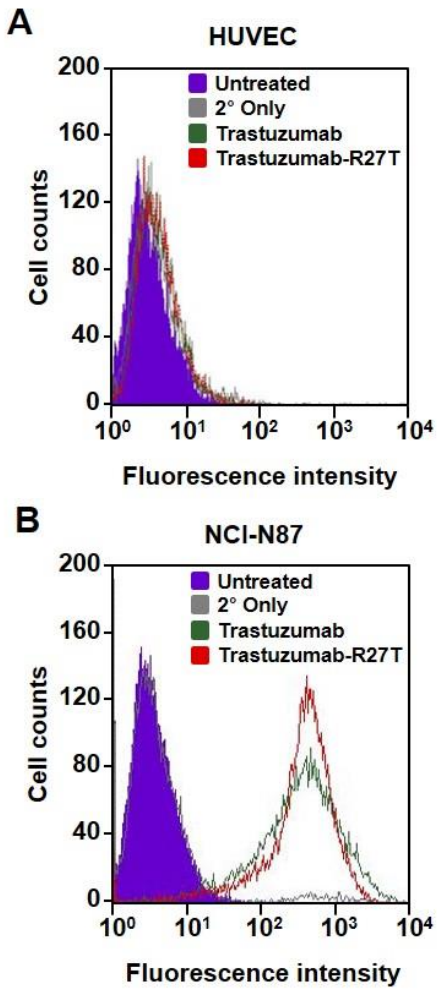

Figure 7. Analysis of ERBB-2-targeting function by FACS. HUVECs (A) and NCI-N87 cells (B) were stained with trastuzumab or trantuzumab-R27T, and fluorescence-positive cells were measured by flow cytometry.

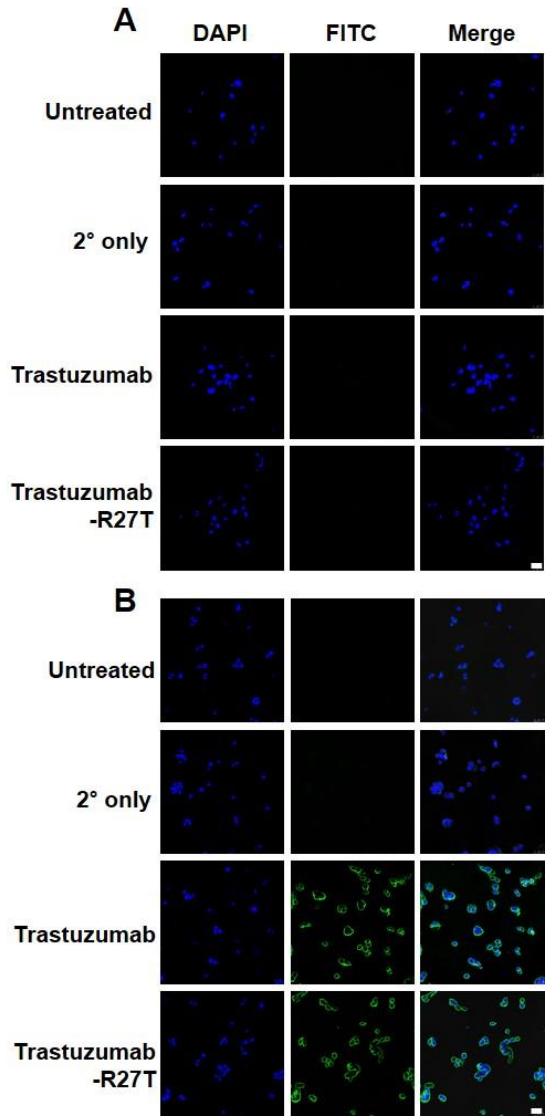

Figure 8. Analysis of ERBB-2-targeting function by confocal microscopy. HUVECs (A) and NCI-N87 cells (B) were incubated with trastuzumab or trantuzumab-R27T for 1 h, and cellular fluorescence was observed by confocal microscopy.

6. *In vitro* anti-cancer efficacy of trastuzumab-R27T

I next examined the *in vitro* anti-cancer efficacy of trastuzumab-R27T. To test its direct efficacy, HUVECs or NCI-N87 cells were treated with R27T, trastuzumab, or the fusion protein. In the WST assay system, treatment with R27T or the fusion protein reduced NCI-N87 viability to 56.8% ± 3.3% and 59.2% ± 2%, respectively (Figure 9A). Similarly, fluorescent microscopy revealed that the smallest live-cell populations were observed in cultures treated with R27T or the fusion protein (Figure 9B).

I further verified the effect of the fusion protein on CDC and ADCC. Neither trastuzumab nor the fusion protein showed CDC efficacy in ERBB-2- (HUVEC) or ERBB-2+ (NCI-N87) cells (Figure 10). However, both agents triggered similar maximum ADCC effects in NCI-N87 cells (76.8% ± 0.2% and 77.1% ± 0.2% cell lysis, respectively, at 1000 ng/mL) (Figure 11B).

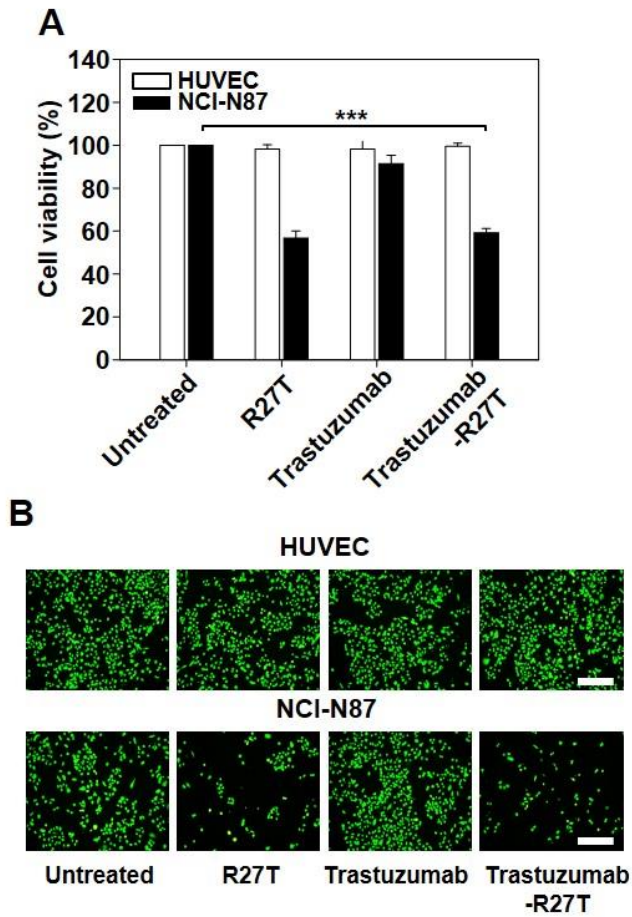

Figure 9. *In vitro* direct anti-cancer efficacy of trastuzumab-R27T. HUVECs and NCI-N87 cells were treated with or without 100 ng/mL of R27T, trastuzumab, or trastuzumab-R27T for 72 h, and cell viability was measured by WST assay (A). Data are presented as the mean ± SD of three independent experiments (***$P < 0.001$ between two groups). (B) Seventy-two hours after treatment, live cells were stained with calcein-AM and analyzed by fluorescence microscopy. Scale bar = 250 μm.

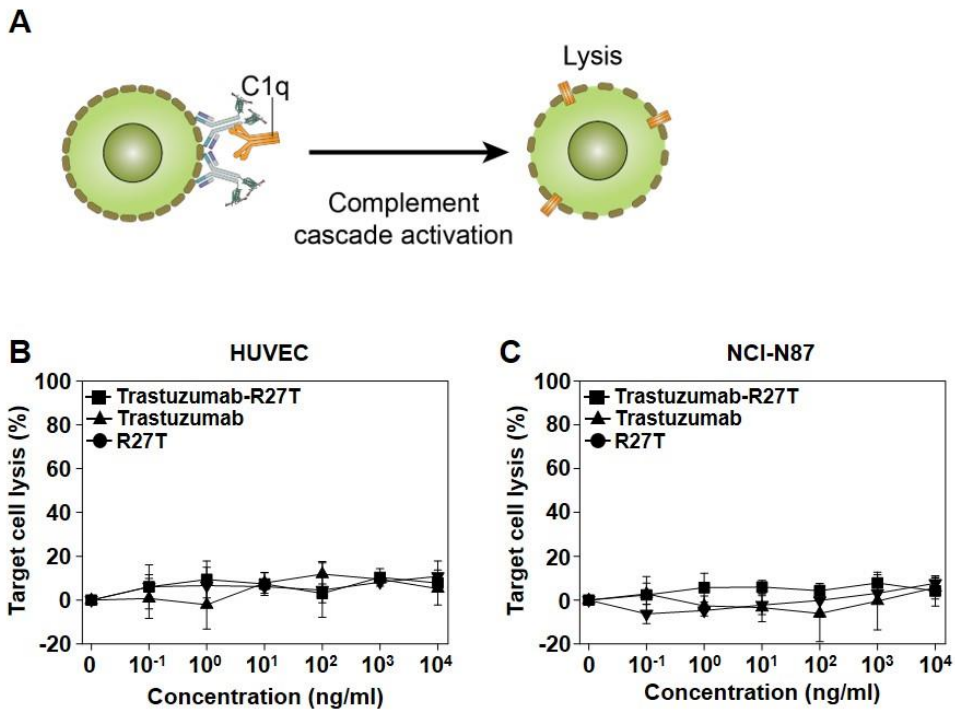

Figure 10. ***In vitro*** **CDC efficacy of trastuzumab-R27T.** (A) The graphical explanation of CDC. HUVECs (B) and NCI-N87 cells (C) were incubated with serial dilutions of R27T, trastuzumab, or trastuzumab-R27T in the presence of 20% human serum (v/v) for 6 h, and viable cells were quantified with the WST assay.

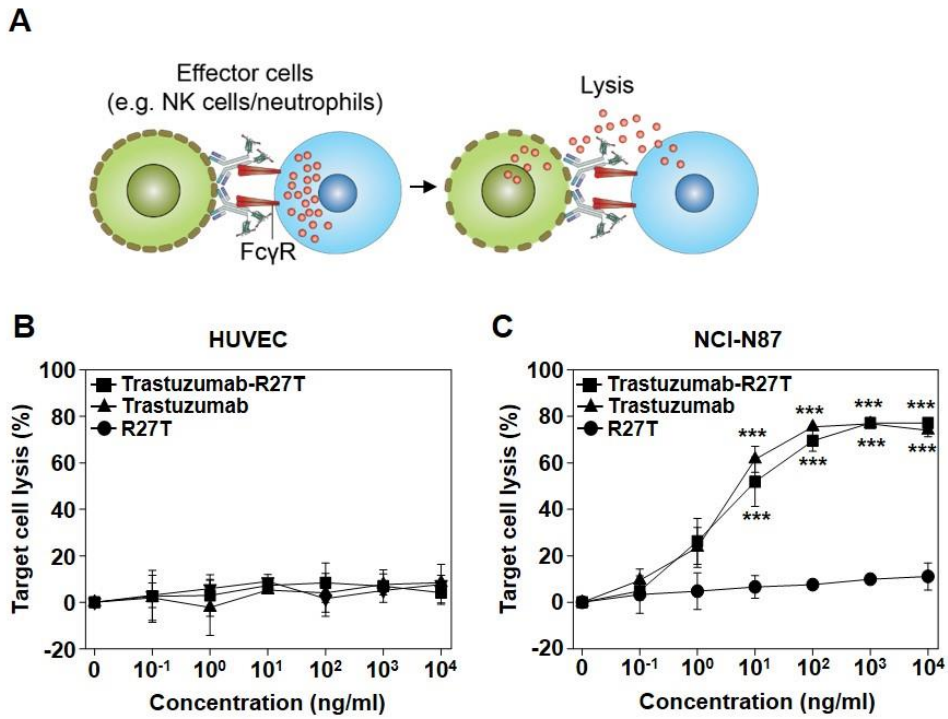

Figure 11. ***In vitro*** **ADCC efficacy of trastuzumab-R27T.** (A) The graphical explanation of ADCCC. HUVECs (B) and NCI-N87 cells (C) were incubated with serial dilutions of R27T, trastuzumab, or trastuzumab-R27T in the presence of NK-92MI-CD16 for 6 h, and viable cells were quantified with the WST assay. The effector/target (E/T) ratio was 8. Error bars indicate the SD of experiments performed in triplicate (***$P < 0.001$ compared to the R27T-treated group).

Discussion

I developed an antibody-cytokine fusion protein comprising a glycoengineered version of recombinant human IFNβ-1a (R27T) linked to the C-terminus of trastuzumab heavy chain, and evaluated its potential for therapeutic use against gastric cancer. Our results showed that the trastuzumab-R27T fusion protein properly induced IFN signaling and direct cytotoxicity. I also found that the fusion protein maintained its ERBB-2-targeting function, as confirmed by FACS and confocal microscopy, and I evaluated the antibody-mediated efficacies (ADCC, CDC) of trastuzumab-R27T.

As the therapeutic use of free IFNs has been limited by a dose-limiting systemic toxicity that makes it impossible deliver optimal concentrations deep into tumor tissues, thus the true therapeutic potential of IFN has not been fully exploited [158]. The use of cancer-targeting molecules to deliver IFN to tumors could facilitate the application of IFN in anti-cancer therapeutics. Furthermore, targeted IFN therapies can activate various immune effector cells (e.g., T cells, dendritic cells, NK cells, and macrophages) that might serve to bridge innate and adaptive anti-tumor immune responses [153-155]. Yang et al. previously reported that anti-EGFR-IFNβ could control EGFR antibody resistance by re-bridging suppressed innate and adaptive immunity in the tumor microenvironment; anti-EGFR-IFNβ stimulated intratumoral

dendritic cells, which reactivated cytotoxic T-cells by increasing antigen cross-presentation within the tumor microenvironment [22]. Since several groups previously reported that ERBB-2-targeted therapies require both type I and type II IFN immunostimulatory responses [21, 44], I chose trastuzumab as a fusion partner for R27T. I believe that a fused version of trastuzumab and R27T might prove to be a powerful therapeutic candidate for ERBB-2-targeted therapy.

Various approaches may be used to fuse a cytokine to an antibody. The domain structure of an antibody facilitates molecular engineering can be used to fuse a cytokine to a full IgG or IgG fragments, such as Fab or scFv [159, 160]. Here, I fused R27T to the C-terminus of the trastuzumab heavy chain. Since IFNβ, IFNAR1, and IFNAR2 form a ternary complex [161], I determined that using the C-terminus of the heavy chain which would facilitate the flexible access of trastuzumab-fused R27T to interferon receptors.

It is notable that the R27T fusion protein showed a 6-fold higher expression level than the corresponding wild-type IFNβ-1a fusion protein in CHO cells (Figure 3B). To explore the mechanistic basis of this finding, I examined the expression levels of heavy chain-IFNβ-1a, heavy chian-R27T, and LC in lysates from expression vector transfected CHO cells. Surprisingly, the expression level of HC-IFNβ-1a was higher than that of HC-R27T (Figure 3C). I therefore speculate that IFNβ-1a-fused trastuzumab suffers from some

issue with insufficient protein assembly, poor protein export, and/or degradation compared to the R27T fusion protein.

Dynamic light scattering revealed that the size of trastuzumab-R27T was approximately 16.8 nm (Figure 4B). Previous studies reported that R27T had a size distribution peak at around 3.7 nm [107] and that trastuzumab maintained a size of 11.4 nm over a 28-day period, even at a high concentration [157]. Therefore, the fusion of trastuzumab with R27T resulted in a size increase relative to the sum of their individual sizes. Moreover, the trastuzumab tended to form β-sheet secondary structures, with a β-sheet content of 29.86% (Figure 5E). Our observations are consistent with a previous report that trastuzumab showed a dominance of β-sheet secondary structural conformation [157]. The α-helix content of trastuzumab-R27T was 9.85% higher than that of trastuzumab (Figure 5F). Prior studies found that R27T contains more α-helices and less β-sheet than rhRFN-β [107, 162].

In concordance with earlier reports [163, 164], I did not observe any CDC-mediated cytolytic effect of trastuzumab or trastuzumab-R27T against NCI-N87 cells, even at 10 μg/mL (Figure 10). As expected, the trastuzumab-R27T fusion protein maintained the ADCC effect of trastuzumab (Figure 11B).

Conclusions and Perspectives

Type I IFNs are expressed in a broad range of mammalian cells and have been considered potential anti-cancer therapeutic candidates because they are related to various protective mechanisms, such as intercellular anti-viral, anti-proliferation, anti-angiogenic, and immune control, through interferon receptor-mediated signal transductions. US FDA approved IFNα as anti-cancer therapeutic agent against chronic myeloid leukemia, melanoma, and renal cell carcinoma in 1988; however, its therapeutic use has reduced recently because of side effects, non-responsiveness, and development of tolerance [158].

Currently, various studies have shown the anti-cancer effect of IFNβ, which has been verified by the several hundred times higher therapeutic response compared to that of IFNα [165, 166]. Furthermore, several clinical studies on the application of IFNβ are in progress. However, IFNβ showed inefficient *Escherichia coli* based protein expression and the activities of *Escherichia coli* expressed IFNβ were significantly low. Active IFNβ should be produced in animal cells; however, the production efficiency was quite low compared to that for other proteins. These factors may slow down the anti-cancer application of IFNβ despite its high therapeutic effect. To overcome these limitations of IFNβ, our lab has developed a glycoengineered IFNβ, R27T. R27T exhibited superior stability, solubility, productivity, and pharmacokinetic properties without loss of biological activity and alteration in receptor binding affinity.

Although the protein productivity and stability are improved, R27T has the limitation of resistance. To overcome R27T resistance, I developed a co-treatment strategy by blocking cFLIP. Since cFLIP has a structure similar to caspase-8, developing a small molecule targeting cFLIP was impossible [115]. Several studies have reported agents that reduce cFLIP expression, thus affecting the transcription, degradation, and translation of cFLIP [115, 167]. Among these agents, I selected two strategies, of which one was that of siRNA for specific inhibition of cFLIP and the other was that of a small molecule targeting CK-II, the upstream molecule of cFLIP responsible for transcription and stability of cFLIP. Results suggested that R27T has potential as an anti-cancer drug, and that a combination therapy using R27T and cFLIP inhibitors might be an effective strategy for overcoming R27T resistance. For further study, in vivo synergistic efficacy of R27T and cFLIP siRNA will be confirmed.

However, therapies using R27T alone could induce severe side effects, resulting from absorption of R27T in the peripheral tissues before reaching the tumor site. To overcome these limitations, I developed a trastuzumab-R27T fusion protein. The fusion protein utilizes the tumor-targeting ability of trastuzumab to lead R27T specifically to ERBB-2-overexpressing tumor tissues and may stimulates enhanced anti-tumor immune responses in a tumor microenvironment while mitigating systemic toxicities.

A known IFNβ mediated anti-cancer response is the activation of

dendritic cells, promotion of cancer antigen cross-presentation and activation of cancer specific CD8+ T cells through these mechanisms [156, 158]. According to a recent report, though there is exception, over 80 % of immune checkpoint blockages including those by anti-PD1 and anti-CTLA4 antibodies led to no response in patients and was attributed to the number of cancer neoantigens [168]. A low neoantigen level is not sufficient to recruit T cells to cancerous tissue. IFNβ can improve antigen presentation ability of dendritic cells, and in cancer cells, IFNβ treatment upregulates PD-L1 expression. Thus, the combination therapy is expected to exert powerful synergistic effects of IFNβ with immune checkpoint inhibitors such as anti-PD1 or -PD-L1 in low neoantigen patients. Additionally, this therapy is expected to overcome the issue of non-response in patients, which IFNβ and immune checkpoint blockade therapies previously encountered.

Therefore, the combination therapy comprising the antibody-R27T fusion protein, cFLIP inhibitor, and immune checkpoint blockers will be a promising strategy to treat cancer patients in the future.

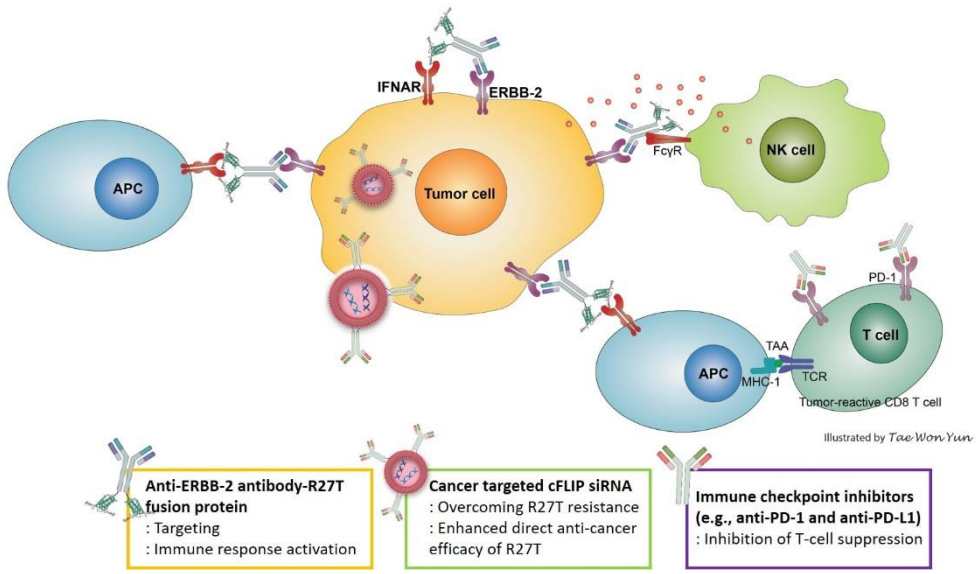

Figure 1. Strategy for combination therapy. Combination therapy comprising the antibody-R27T fusion protein, cFLIP siRNA, and immune checkpoint blockers.

References

1. Parker BS, Rautela J and Hertzog PJ. Antitumour actions of interferons: implications for cancer therapy. Nat Rev Cancer. 2016; 16: 131-144.

2. Platanias LC. Mechanisms of type-I- and type-II-interferon-mediated signalling. Nat Rev Immunol. 2005; 5: 375-386.

3. Schoggins JW and Rice CM. Interferon-stimulated genes and their antiviral effector functions. Curr Opin Virol. 2011; 1: 519-525.

4. Bekisz J, Baron S, Balinsky C, Morrow A and Zoon KC. Antiproliferative Properties of Type I and Type II Interferon. Pharmaceuticals. 2010; 3: 994-1015.

5. Lindner DJ. Interferons as antiangiogenic agents. Curr Oncol Rep. 2002; 4: 510-514.

6. Bekisz J, Sato Y, Johnson C, Husain SR, Puri RK and Zoon KC. Immunomodulatory effects of interferons in malignancies. J Interferon Cytokine Res. 2013; 33: 154-161.

7. Sandoval R, Xue J, Pilkinton M, Salvi D, Kiyokawa H and Colamonici OR. Different requirements for the cytostatic and apoptotic effects of type I interferons. Induction of apoptosis requires ARF but not p53 in osteosarcoma cell lines. J Biol Chem. 2004; 279: 32275-32280.

8. Vitale G, van Eijck CH, van Koetsveld Ing PM, Erdmann JI, Speel EJ, van der Wansem Ing K, Mooij DM, Colao A, Lombardi G, Croze E, Lamberts SW and Hofland LJ. Type I interferons in the treatment of pancreatic cancer: mechanisms of action and role of related receptors. Ann Surg. 2007; 246: 259-268.

9. Chawla-Sarkar M, Lindner DJ, Liu YF, Williams BR, Sen GC, Silverman RH and Borden EC. Apoptosis and interferons: role of interferon-stimulated

genes as mediators of apoptosis. Apoptosis. 2003; 8: 237-249.
10. Caraglia M, Marra M, Tagliaferri P, Lamberts SW, Zappavigna S, Misso G, Cavagnini F, Facchini G, Abbruzzese A, Hofland LJ and Vitale G. Emerging strategies to strengthen the anti-tumour activity of type I interferons: overcoming survival pathways. Curr Cancer Drug Targets. 2009; 9: 690-704.
11. Hakansson A, Gustafsson B, Krysander L and Hakansson L. Tumour-infiltrating lymphocytes in metastatic malignant melanoma and response to interferon alpha treatment. Br J Cancer. 1996; 74: 670-676.
12. Fellous M, Nir U, Wallach D, Merlin G, Rubinstein M and Revel M. Interferon-dependent induction of mRNA for the major histocompatibility antigens in human fibroblasts and lymphoblastoid cells. Proc Natl Acad Sci U S A. 1982; 79: 3082-3086.
13. Khallouf H, Marten A, Serba S, Teichgraber V, Buchler MW, Jager D and Schmidt J. 5-Fluorouracil and interferon-alpha immunochemotherapy enhances immunogenicity of murine pancreatic cancer through upregulation of NKG2D ligands and MHC class I. J Immunother. 2012; 35: 245-253.
14. Raig ET, Jones NB, Varker KA, Benniger K, Go MR, Biber JL, Lesinski GB and Carson WE, 3rd. VEGF secretion is inhibited by interferon-alpha in several melanoma cell lines. J Interferon Cytokine Res. 2008; 28: 553-561.
15. Lindner DJ and Borden EC. Effects of tamoxifen and interferon-beta or the combination on tumor-induced angiogenesis. Int J Cancer. 1997; 71: 456-461.
16. von Marschall Z, Scholz A, Cramer T, Schafer G, Schirner M, Oberg K, Wiedenmann B, Hocker M and Rosewicz S. Effects of interferon alpha on vascular endothelial growth factor gene transcription and tumor angiogenesis. J Natl Cancer Inst. 2003; 95: 437-448.
17. Singh RK, Gutman M, Bucana CD, Sanchez R, Llansa N and Fidler IJ.

Interferons alpha and beta down-regulate the expression of basic fibroblast growth factor in human carcinomas. Proc Natl Acad Sci U S A. 1995; 92: 4562-4566.
18. Weiss K. Safety profile of interferon-alpha therapy. Semin Oncol. 1998; 25: 9-13.
19. Chelbi-Alix MK and Wietzerbin J. Interferon, a growing cytokine family: 50 years of interferon research. Biochimie. 2007; 89: 713-718.
20. Zitvogel L, Galluzzi L, Kepp O, Smyth MJ and Kroemer G. Type I interferons in anticancer immunity. Nat Rev Immunol. 2015; 15: 405-414.
21. Stagg J, Loi S, Divisekera U, Ngiow SF, Duret H, Yagita H, Teng MW and Smyth MJ. Anti-ErbB-2 mAb therapy requires type I and II interferons and synergizes with anti-PD-1 or anti-CD137 mAb therapy. Proc Natl Acad Sci U S A. 2011; 108: 7142-7147.
22. Yang X, Zhang X, Fu ML, Weichselbaum RR, Gajewski TF, Guo Y and Fu YX. Targeting the tumor microenvironment with interferon-beta bridges innate and adaptive immune responses. Cancer Cell. 2014; 25: 37-48.
23. Sistigu A, Yamazaki T, Vacchelli E, Chaba K, Enot DP, Adam J, Vitale I, Goubar A, Baracco EE, Remedios C, Fend L, Hannani D, Aymeric L, Ma Y, Niso-Santano M, Kepp O, et al. Cancer cell-autonomous contribution of type I interferon signaling to the efficacy of chemotherapy. Nat Med. 2014; 20: 1301-1309.
24. Dunn GP, Bruce AT, Ikeda H, Old LJ and Schreiber RD. Cancer immunoediting: from immunosurveillance to tumor escape. Nat Immunol. 2002; 3: 991-998.
25. Shankaran V, Ikeda H, Bruce AT, White JM, Swanson PE, Old LJ and Schreiber RD. IFNgamma and lymphocytes prevent primary tumour development and shape tumour immunogenicity. Nature. 2001; 410: 1107-

1111.
26. Kaplan DH, Shankaran V, Dighe AS, Stockert E, Aguet M, Old LJ and Schreiber RD. Demonstration of an interferon gamma-dependent tumor surveillance system in immunocompetent mice. Proc Natl Acad Sci U S A. 1998; 95: 7556-7561.
27. Noser JA, Mael AA, Sakuma R, Ohmine S, Marcato P, Lee PW and Ikeda Y. The RAS/Raf1/MEK/ERK signaling pathway facilitates VSV-mediated oncolysis: implication for the defective interferon response in cancer cells. Mol Ther. 2007; 15: 1531-1536.
28. Sexl V, Kovacic B, Piekorz R, Moriggl R, Stoiber D, Hoffmeyer A, Liebminger R, Kudlacek O, Weisz E, Rothammer K and Ihle JN. Jak1 deficiency leads to enhanced Abelson-induced B-cell tumor formation. Blood. 2003; 101: 4937-4943.
29. Cheon H, Holvey-Bates EG, Schoggins JW, Forster S, Hertzog P, Imanaka N, Rice CM, Jackson MW, Junk DJ and Stark GR. IFNbeta-dependent increases in STAT1, STAT2, and IRF9 mediate resistance to viruses and DNA damage. EMBO J. 2013; 32: 2751-2763.
30. Yang J and Stark GR. Roles of unphosphorylated STATs in signaling. Cell Res. 2008; 18: 443-451.
31. Kumar KG, Tang W, Ravindranath AK, Clark WA, Croze E and Fuchs SY. SCF(HOS) ubiquitin ligase mediates the ligand-induced down-regulation of the interferon-alpha receptor. EMBO J. 2003; 22: 5480-5490.
32. Leyva L, Fernandez O, Fedetz M, Blanco E, Fernandez VE, Oliver B, Leon A, Pinto-Medel MJ, Mayorga C, Guerrero M, Luque G, Alcina A and Matesanz F. IFNAR1 and IFNAR2 polymorphisms confer susceptibility to multiple sclerosis but not to interferon-beta treatment response. J Neuroimmunol. 2005; 163: 165-171.

33. Mizukoshi E, Kaneko S, Kaji K, Terasaki S, Matsushita E, Muraguchi M, Ohmoto Y and Kobayashi K. Serum levels of soluble interferon Alfa/Beta receptor as an inhibitory factor of interferon in the patients with chronic hepatitis C. Hepatology. 1999; 30: 1325-1331.
34. Hardy MP, Owczarek CM, Trajanovska S, Liu X, Kola I and Hertzog PJ. The soluble murine type I interferon receptor Ifnar-2 is present in serum, is independently regulated, and has both agonistic and antagonistic properties. Blood. 2001; 97: 473-482.
35. Xiang Z, Zhao Y, Mitaksov V, Fremont DH, Kasai Y, Molitoris A, Ries RE, Miner TL, McLellan MD, DiPersio JF, Link DC, Payton JE, Graubert TA, Watson M, Shannon W, Heath SE, et al. Identification of somatic JAK1 mutations in patients with acute myeloid leukemia. Blood. 2008; 111: 4809-4812.
36. Flex E, Petrangeli V, Stella L, Chiaretti S, Hornakova T, Knoops L, Ariola C, Fodale V, Clappier E, Paoloni F, Martinelli S, Fragale A, Sanchez M, Tavolaro S, Messina M, Cazzaniga G, et al. Somatically acquired JAK1 mutations in adult acute lymphoblastic leukemia. J Exp Med. 2008; 205: 751-758.
37. Ren Y, Zhang Y, Liu RZ, Fenstermacher DA, Wright KL, Teer JK and Wu J. JAK1 truncating mutations in gynecologic cancer define new role of cancer-associated protein tyrosine kinase aberrations. Sci Rep. 2013; 3: 3042.
38. Du Z, Wei L, Murti A, Pfeffer SR, Fan M, Yang CH and Pfeffer LM. Non-conventional signal transduction by type 1 interferons: the NF-kappaB pathway. J Cell Biochem. 2007; 102: 1087-1094.
39. Critchley-Thorne RJ, Simons DL, Yan N, Miyahira AK, Dirbas FM, Johnson DL, Swetter SM, Carlson RW, Fisher GA, Koong A, Holmes S and Lee PP. Impaired interferon signaling is a common immune defect in human

cancer. Proc Natl Acad Sci U S A. 2009; 106: 9010-9015.
40. Alexander WS. Suppressors of cytokine signalling (SOCS) in the immune system. Nat Rev Immunol. 2002; 2: 410-416.
41. Wong LH, Krauer KG, Hatzinisiriou I, Estcourt MJ, Hersey P, Tam ND, Edmondson S, Devenish RJ and Ralph SJ. Interferon-resistant human melanoma cells are deficient in ISGF3 components, STAT1, STAT2, and p48-ISGF3gamma. J Biol Chem. 1997; 272: 28779-28785.
42. Kirkwood J. Cancer immunotherapy: the interferon-alpha experience. Semin Oncol. 2002; 29: 18-26.
43. Mattarollo SR, Loi S, Duret H, Ma Y, Zitvogel L and Smyth MJ. Pivotal role of innate and adaptive immunity in anthracycline chemotherapy of established tumors. Cancer Res. 2011; 71: 4809-4820.
44. Hannesdottir L, Tymoszuk P, Parajuli N, Wasmer MH, Philipp S, Daschil N, Datta S, Koller JB, Tripp CH, Stoitzner P, Muller-Holzner E, Wiegers GJ, Sexl V, Villunger A and Doppler W. Lapatinib and doxorubicin enhance the Stat1-dependent antitumor immune response. Eur J Immunol. 2013; 43: 2718-2729.
45. Slaney CY, Rautela J and Parker BS. The emerging role of immunosurveillance in dictating metastatic spread in breast cancer. Cancer Res. 2013; 73: 5852-5857.
46. Pardoll DM. The blockade of immune checkpoints in cancer immunotherapy. Nat Rev Cancer. 2012; 12: 252-264.
47. Formenti SC and Demaria S. Systemic effects of local radiotherapy. Lancet Oncol. 2009; 10: 718-726.
48. Demaria S, Pilones KA, Vanpouille-Box C, Golden EB and Formenti SC. The optimal partnership of radiation and immunotherapy: from preclinical studies to clinical translation. Radiat Res. 2014; 182: 170-181.

49. Liu Y, Carlsson R, Ambjorn M, Hasan M, Badn W, Darabi A, Siesjo P and Issazadeh-Navikas S. PD-L1 expression by neurons nearby tumors indicates better prognosis in glioblastoma patients. J Neurosci. 2013; 33: 14231-14245.

50. Micheau O. Cellular FLICE-inhibitory protein: an attractive therapeutic target? Expert Opin Ther Targets. 2003; 7: 559-573.

51. Irmler M, Thome M, Hahne M, Schneider P, Hofmann K, Steiner V, Bodmer JL, Schroter M, Burns K, Mattmann C, Rimoldi D, French LE and Tschopp J. Inhibition of death receptor signals by cellular FLIP. Nature. 1997; 388: 190-195.

52. Chang L, Kamata H, Solinas G, Luo JL, Maeda S, Venuprasad K, Liu YC and Karin M. The E3 ubiquitin ligase itch couples JNK activation to TNFalpha-induced cell death by inducing c-FLIP(L) turnover. Cell. 2006; 124: 601-613.

53. Micheau O, Thome M, Schneider P, Holler N, Tschopp J, Nicholson DW, Briand C and Grutter MG. The long form of FLIP is an activator of caspase-8 at the Fas death-inducing signaling complex. J Biol Chem. 2002; 277: 45162-45171.

54. Krueger A, Baumann S, Krammer PH and Kirchhoff S. FLICE-inhibitory proteins: regulators of death receptor-mediated apoptosis. Mol Cell Biol. 2001; 21: 8247-8254.

55. Hernandez A, Wang QD, Schwartz SA and Evers BM. Sensitization of human colon cancer cells to TRAIL-mediated apoptosis. J Gastrointest Surg. 2001; 5: 56-65.

56. Elnemr A, Ohta T, Yachie A, Kayahara M, Kitagawa H, Fujimura T, Ninomiya I, Fushida S, Nishimura GI, Shimizu K and Miwa K. Human pancreatic cancer cells disable function of Fas receptors at several levels in

Fas signal transduction pathway. Int J Oncol. 2001; 18: 311-316.
57. Nam SY, Jung GA, Hur GC, Chung HY, Kim WH, Seol DW and Lee BL. Upregulation of FLIP(S) by Akt, a possible inhibition mechanism of TRAIL-induced apoptosis in human gastric cancers. Cancer Sci. 2003; 94: 1066-1073.
58. Xiao CW, Yan X, Li Y, Reddy SA and Tsang BK. Resistance of human ovarian cancer cells to tumor necrosis factor alpha is a consequence of nuclear factor kappaB-mediated induction of Fas-associated death domain-like interleukin-1beta-converting enzyme-like inhibitory protein. Endocrinology. 2003; 144: 623-630.
59. Zhang X, Jin TG, Yang H, DeWolf WC, Khosravi-Far R and Olumi AF. Persistent c-FLIP(L) expression is necessary and sufficient to maintain resistance to tumor necrosis factor-related apoptosis-inducing ligand-mediated apoptosis in prostate cancer. Cancer Res. 2004; 64: 7086-7091.
60. Korkolopoulou P, Goudopoulou A, Voutsinas G, Thomas-Tsagli E, Kapralos P, Patsouris E and Saetta AA. c-FLIP expression in bladder urothelial carcinomas: its role in resistance to Fas-mediated apoptosis and clinicopathologic correlations. Urology. 2004; 63: 1198-1204.
61. Zong H, Yin B, Chen J, Ma B, Cai D and He X. Over-expression of c-FLIP confers the resistance to TRAIL-induced apoptosis on gallbladder carcinoma. Tohoku J Exp Med. 2009; 217: 203-208.
62. Salon C, Eymin B, Micheau O, Chaperot L, Plumas J, Brambilla C, Brambilla E and Gazzeri S. E2F1 induces apoptosis and sensitizes human lung adenocarcinoma cells to death-receptor-mediated apoptosis through specific downregulation of c-FLIP(short). Cell Death Differ. 2006; 13: 260-272.
63. Wilson NS, Dixit V and Ashkenazi A. Death receptor signal transducers: nodes of coordination in immune signaling networks. Nat Immunol. 2009; 10:

348-355.
64. Okano H, Shiraki K, Inoue H, Kawakita T, Yamanaka T, Deguchi M, Sugimoto K, Sakai T, Ohmori S, Fujikawa K, Murata K and Nakano T. Cellular FLICE/caspase-8-inhibitory protein as a principal regulator of cell death and survival in human hepatocellular carcinoma. Lab Invest. 2003; 83: 1033-1043.
65. Lee SH, Kim HS, Kim SY, Lee YS, Park WS, Kim SH, Lee JY and Yoo NJ. Increased expression of FLIP, an inhibitor of Fas-mediated apoptosis, in stomach cancer. APMIS. 2003; 111: 309-314.
66. Zhou XD, Yu JP, Liu J, Luo HS, Chen HX and Yu HG. Overexpression of cellular FLICE-inhibitory protein (FLIP) in gastric adenocarcinoma. Clin Sci. 2004; 106: 397-405.
67. Bullani RR, Huard B, Viard-Leveugle I, Byers HR, Irmler M, Saurat JH, Tschopp J and French LE. Selective expression of FLIP in malignant melanocytic skin lesions. J Invest Dermatol. 2001; 117: 360-364.
68. Djerbi M, Screpanti V, Catrina AI, Bogen B, Biberfeld P and Grandien A. The inhibitor of death receptor signaling, FLICE-inhibitory protein defines a new class of tumor progression factors. J Exp Med. 1999; 190: 1025-1032.
69. Kelso A. Cytokines: principles and prospects. Immunol Cell Biol. 1998; 76: 300-317.
70. Ardolino M, Hsu J and Raulet DH. Cytokine treatment in cancer immunotherapy. Oncotarget. 2015; 6: 19346-19347.
71. Mocellin S, Wang E and Marincola FM. Cytokines and immune response in the tumor microenvironment. J Immunother. 2001; 24: 392-407.
72. Fewkes NM and Mackall CL. Novel gamma-chain cytokines as candidate immune modulators in immune therapies for cancer. Cancer J. 2010; 16: 392-398.

73. Jonasch E and Haluska FG. Interferon in oncological practice: review of interferon biology, clinical applications, and toxicities. Oncologist. 2001; 6: 34-55.
74. Baldo BA. Side effects of cytokines approved for therapy. Drug Saf. 2014; 37: 921-943.
75. Ortiz-Sanchez E, Helguera G, Daniels TR and Penichet ML. Antibody-cytokine fusion proteins: applications in cancer therapy. Expert Opin Biol Ther. 2008; 8: 609-632.
76. Lechner MG, Russell SM, Bass RS and Epstein AL. Chemokines, costimulatory molecules and fusion proteins for the immunotherapy of solid tumors. Immunotherapy. 2011; 3: 1317-1340.
77. Helguera G and Penichet ML. Antibody-cytokine fusion proteins for the therapy of cancer. Methods Mol Med. 2005; 109: 347-374.
78. Helguera G, Morrison SL and Penichet ML. Antibody-cytokine fusion proteins: harnessing the combined power of cytokines and antibodies for cancer therapy. Clin Immunol. 2002; 105: 233-246.
79. Mujoo K, Cheresh DA, Yang HM and Reisfeld RA. Disialoganglioside GD2 on human neuroblastoma cells: target antigen for monoclonal antibody-mediated cytolysis and suppression of tumor growth. Cancer Res. 1987; 47: 1098-1104.
80. Becker JC, Pancook JD, Gillies SD, Mendelsohn J and Reisfeld RA. Eradication of human hepatic and pulmonary melanoma metastases in SCID mice by antibody-interleukin 2 fusion proteins. Proc Natl Acad Sci U S A. 1996; 93: 2702-2707.
81. Albertini MR, Hank JA, Gadbaw B, Kostlevy J, Haldeman J, Schalch H, Gan J, Kim K, Eickhoff J, Gillies SD and Sondel PM. Phase II trial of hu14.18-IL2 for patients with metastatic melanoma. Cancer Immunol

Immunother. 2012; 61: 2261-2271.
82. Shusterman S, London WB, Gillies SD, Hank JA, Voss SD, Seeger RC, Reynolds CP, Kimball J, Albertini MR, Wagner B, Gan J, Eickhoff J, DeSantes KB, Cohn SL, Hecht T, Gadbaw B, et al. Antitumor activity of hu14.18-IL2 in patients with relapsed/refractory neuroblastoma: a Children's Oncology Group (COG) phase II study. J Clin Oncol. 2010; 28: 4969-4975.
83. Gillies SD, Lan Y, Williams S, Carr F, Forman S, Raubitschek A and Lo KM. An anti-CD20-IL-2 immunocytokine is highly efficacious in a SCID mouse model of established human B lymphoma. Blood. 2005; 105: 3972-3978.
84. Rossi EA, Goldenberg DM, Cardillo TM, Stein R and Chang CH. CD20-targeted tetrameric interferon-alpha, a novel and potent immunocytokine for the therapy of B-cell lymphomas. Blood. 2009; 114: 3864-3871.
85. Xuan C, Steward KK, Timmerman JM and Morrison SL. Targeted delivery of interferon-alpha via fusion to anti-CD20 results in potent antitumor activity against B-cell lymphoma. Blood. 2010; 115: 2864-2871.
86. Bhatt S ZD, Jiang X, Shin SU, Timmerman JM, Rosenblatt JD and Lossos IS. Targeting B-Cell Malignancies With Anti-CD20-Interleukin-21 Fusokine. Blood. 2013; 377.
87. Rossi EA, Rossi DL, Cardillo TM, Stein R, Goldenberg DM and Chang CH. Preclinical studies on targeted delivery of multiple IFNalpha2b to HLA-DR in diverse hematologic cancers. Blood. 2011; 118: 1877-1884.
88. Gillessen S, Gnad-Vogt US, Gallerani E, Beck J, Sessa C, Omlin A, Mattiacci MR, Liedert B, Kramer D, Laurent J, Speiser DE and Stupp R. A phase I dose-escalation study of the immunocytokine EMD 521873 (Selectikine) in patients with advanced solid tumours. Eur J Cancer. 2013; 49: 35-44.

89. Laurent J, Touvrey C, Gillessen S, Joffraud M, Vicari M, Bertrand C, Ongarello S, Liedert B, Gallerani E, Beck J, Omlin A, Sessa C, Quaratino S, Stupp R, Gnad-Vogt US and Speiser DE. T-cell activation by treatment of cancer patients with EMD 521873 (Selectikine), an IL-2/anti-DNA fusion protein. J Transl Med. 2013; 11: 5.
90. Kim JW HC, Bilusic M, Singh NK, Madan RA, Sabzevari H, Schlom J, Gulley JL. First-in-human phase I trial of NHS-IL12 in advanced solid tumors. J Clin Oncol 2012; 30: 2012.
91. Marlind J, Kaspar M, Trachsel E, Sommavilla R, Hindle S, Bacci C, Giovannoni L and Neri D. Antibody-mediated delivery of interleukin-2 to the stroma of breast cancer strongly enhances the potency of chemotherapy. Clin Cancer Res. 2008; 14: 6515-6524.
92. Gutbrodt KL, Schliemann C, Giovannoni L, Frey K, Pabst T, Klapper W, Berdel WE and Neri D. Antibody-based delivery of interleukin-2 to neovasculature has potent activity against acute myeloid leukemia. Sci Transl Med. 2013; 5: 201ra118.
93. Pedretti M, Verpelli C, Marlind J, Bertani G, Sala C, Neri D and Bello L. Combination of temozolomide with immunocytokine F16-IL2 for the treatment of glioblastoma. Br J Cancer. 2010; 103: 827-836.
94. Fowler N and Younes A. There will be blood: targeting tumor vasculature. Blood. 2009; 113: 2121-2122.
95. Schliemann C, Palumbo A, Zuberbuhler K, Villa A, Kaspar M, Trachsel E, Klapper W, Menssen HD and Neri D. Complete eradication of human B-cell lymphoma xenografts using rituximab in combination with the immunocytokine L19-IL2. Blood. 2009; 113: 2275-2283.
96. Eigentler TK, Weide B, de Braud F, Spitaleri G, Romanini A, Pflugfelder A, Gonzalez-Iglesias R, Tasciotti A, Giovannoni L, Schwager K, Lovato V,

Kaspar M, Trachsel E, Menssen HD, Neri D and Garbe C. A dose-escalation and signal-generating study of the immunocytokine L19-IL2 in combination with dacarbazine for the therapy of patients with metastatic melanoma. Clin Cancer Res. 2011; 17: 7732-7742.

97. Borsi L, Balza E, Carnemolla B, Sassi F, Castellani P, Berndt A, Kosmehl H, Biro A, Siri A, Orecchia P, Grassi J, Neri D and Zardi L. Selective targeted delivery of TNFalpha to tumor blood vessels. Blood. 2003; 102: 4384-4392.

98. Spitaleri G, Berardi R, Pierantoni C, De Pas T, Noberasco C, Libbra C, Gonzalez-Iglesias R, Giovannoni L, Tasciotti A, Neri D, Menssen HD and de Braud F. Phase I/II study of the tumour-targeting human monoclonal antibody-cytokine fusion protein L19-TNF in patients with advanced solid tumours. J Cancer Res Clin Oncol. 2013; 139: 447-455.

99. Papadia F, Basso V, Patuzzo R, Maurichi A, Di Florio A, Zardi L, Ventura E, Gonzalez-Iglesias R, Lovato V, Giovannoni L, Tasciotti A, Neri D, Santinami M, Menssen HD and De Cian F. Isolated limb perfusion with the tumor-targeting human monoclonal antibody-cytokine fusion protein L19-TNF plus melphalan and mild hyperthermia in patients with locally advanced extremity melanoma. J Surg Oncol. 2013; 107: 173-179.

100. Lo KM, Lan Y, Lauder S, Zhang J, Brunkhorst B, Qin G, Verma R, Courtenay-Luck N and Gillies SD. huBC1-IL12, an immunocytokine which targets EDB-containing oncofetal fibronectin in tumors and tumor vasculature, shows potent anti-tumor activity in human tumor models. Cancer Immunol Immunother. 2007; 56: 447-457.

101. Rudman SM, Jameson MB, McKeage MJ, Savage P, Jodrell DI, Harries M, Acton G, Erlandsson F and Spicer JF. A phase 1 study of AS1409, a novel antibody-cytokine fusion protein, in patients with malignant melanoma or renal cell carcinoma. Clin Cancer Res. 2011; 17: 1998-2005.

102. Gladkov O BM, Ramlau R, Serwatowski P, Milanowski J, Tomeczko J, Komarnitsky PB, Bernard L, Kramer D, Krzakowski MJ. Phase II trial of huKS-IL2 with cyclophosphamide (CTX) in patients with extensive disease small-cell lung cancer (ED-SCLC). Journal of Clinical Oncology. 2012; 30: 15.
103. Connor JP, Cristea MC, Lewis NL, Lewis LD, Komarnitsky PB, Mattiacci MR, Felder M, Stewart S, Harter J, Henslee-Downey J, Kramer D, Neugebauer R and Stupp R. A phase 1b study of humanized KS-interleukin-2 (huKS-IL2) immunocytokine with cyclophosphamide in patients with EpCAM-positive advanced solid tumors. BMC Cancer. 2013; 13: 20.
104. Klein C. Novel CEA-targeted IL2 variant immunocytokine for immunotherapy of cancer. J Immunother Cancer. 2014; Suppl 2: I8.
105. Gajewski TF and Corrales L. New perspectives on type I IFNs in cancer. Cytokine Growth Factor Rev. 2015; 26: 175-178.
106. Salmon P, Le Cotonnec JY, Galazka A, Abdul-Ahad A and Darragh A. Pharmacokinetics and pharmacodynamics of recombinant human interferon-beta in healthy male volunteers. J Interferon Cytokine Res. 1996; 16: 759-764.
107. Song K, Yoon IS, Kim NA, Kim DH, Lee J, Lee HJ, Lee S, Choi S, Choi MK, Kim HH, Jeong SH, Son WS, Kim DD and Shin YK. Glycoengineering of interferon-beta 1a improves its biophysical and pharmacokinetic properties. PLoS One. 2014; 9: e96967.
108. Katsoulidis E, Kaur S and Platanias LC. Deregulation of Interferon Signaling in Malignant Cells. Pharmaceuticals. 2010; 3: 406-418.
109. Tracey L, Streck CJ, Du Z, Williams RF, Pfeffer LM, Nathwani AC and Davidoff AM. NF-kappaB activation mediates resistance to IFN beta in MLL-rearranged acute lymphoblastic leukemia. Leukemia. 2010; 24: 806-812.

110. Ogasawara S, Yano H, Momosaki S, Akiba J, Nishida N, Kojiro S, Moriya F, Ishizaki H, Kuratomi K and Kojiro M. Growth inhibitory effects of IFN-beta on human liver cancer cells in vitro and in vivo. J Interferon Cytokine Res. 2007; 27: 507-516.

111. Jung HS, Erkin OC, Kwon MJ, Kim SH, Jung JI, Oh YK, Her SW, Ju W, Choi YL, Song SY, Kim JK, Kim YD, Shim GY and Shin YK. The synergistic therapeutic effect of cisplatin with Human papillomavirus E6/E7 short interfering RNA on cervical cancer cell lines in vitro and in vivo. Int J Cancer. 2012; 130: 1925-1936.

112. Livak KJ and Schmittgen TD. Analysis of relative gene expression data using real-time quantitative PCR and the 2(-Delta Delta C(T)) Method. Methods. 2001; 25: 402-408.

113. Albanese J, Meterissian S, Kontogiannea M, Dubreuil C, Hand A, Sorba S and Dainiak N. Biologically active Fas antigen and its cognate ligand are expressed on plasma membrane-derived extracellular vesicles. Blood. 1998; 91: 3862-3874.

114. Xu J, Zhou JY and Wu GS. Tumor necrosis factor-related apoptosis-inducing ligand is required for tumor necrosis factor alpha-mediated sensitization of human breast cancer cells to chemotherapy. Cancer Res. 2006; 66: 10092-10099.

115. Safa AR and Pollok KE. Targeting the Anti-Apoptotic Protein c-FLIP for Cancer Therapy. Cancers. 2011; 3: 1639-1671.

116. Bauer JA, Morrison BH, Grane RW, Jacobs BS, Dabney S, Gamero AM, Carnevale KA, Smith DJ, Drazba J, Seetharam B and Lindner DJ. Effects of interferon beta on transcobalamin II-receptor expression and antitumor activity of nitrosylcobalamin. J Natl Cancer Inst. 2002; 94: 1010-1019.

117. Chawla-Sarkar M, Leaman DW and Borden EC. Preferential induction

of apoptosis by interferon (IFN)-beta compared with IFN-alpha2: correlation with TRAIL/Apo2L induction in melanoma cell lines. Clin Cancer Res. 2001; 7: 1821-1831.

118. Takaoka A, Hayakawa S, Yanai H, Stoiber D, Negishi H, Kikuchi H, Sasaki S, Imai K, Shibue T, Honda K and Taniguchi T. Integration of interferon-alpha/beta signalling to p53 responses in tumour suppression and antiviral defence. Nature. 2003; 424: 516-523.

119. Tsuno T, Mejido J, Zhao T, Schmeisser H, Morrow A and Zoon KC. IRF9 is a key factor for eliciting the antiproliferative activity of IFN-alpha. J Immunother. 2009; 32: 803-816.

120. Yoshikawa T, Takata A, Otsuka M, Kishikawa T, Kojima K, Yoshida H and Koike K. Silencing of microRNA-122 enhances interferon-alpha signaling in the liver through regulating SOCS3 promoter methylation. Sci Rep. 2012; 2: 637.

121. Caraccio N, Cuccato S, Pratesi F, Dardano A, Ursino S, Chimenti D, Boldrini L, Materazzi G, Migliorini P and Monzani F. Effect of type I interferon(s) on cell viability and apoptosis in primary human thyrocyte cultures. Thyroid. 2009; 19: 149-155.

122. Katze MG, Fornek JL, Palermo RE, Walters KA and Korth MJ. Innate immune modulation by RNA viruses: emerging insights from functional genomics. Nat Rev Immunol. 2008; 8: 644-654.

123. McIlwain DR, Berger T and Mak TW. Caspase functions in cell death and disease. Cold Spring Harb Perspect Biol. 2013; 5: a008656.

124. Rusch L, Zhou A and Silverman RH. Caspase-dependent apoptosis by 2',5'-oligoadenylate activation of RNase L is enhanced by IFN-beta. J Interferon Cytokine Res. 2000; 20: 1091-1100.

125. Huang H, Xiao T, He L, Ji H and Liu XY. Interferon-beta-armed

oncolytic adenovirus induces both apoptosis and necroptosis in cancer cells. Acta Biochim Biophys Sin. 2012; 44: 737-745.
126. Lavrik IN. Systems biology of death receptor networks: live and let die. Cell Death Dis. 2014; 5: e1259.
127. Guicciardi ME and Gores GJ. Life and death by death receptors. FASEB J. 2009; 23: 1625-1637.
128. Lavrik IN and Krammer PH. Regulation of CD95/Fas signaling at the DISC. Cell Death Differ. 2012; 19: 36-41.
129. Budd RC, Yeh WC and Tschopp J. cFLIP regulation of lymphocyte activation and development. Nat Rev Immunol. 2006; 6: 196-204.
130. Kaminskyy VO, Surova OV, Piskunova T, Zborovskaya IB, Tchevkina EM, Andera L and Zhivotovsky B. Upregulation of c-FLIP-short in response to TRAIL promotes survival of NSCLC cells, which could be suppressed by inhibition of Ca2+/calmodulin signaling. Cell Death Dis. 2013; 4: e522.
131. Fricker N, Beaudouin J, Richter P, Eils R, Krammer PH and Lavrik IN. Model-based dissection of CD95 signaling dynamics reveals both a pro- and antiapoptotic role of c-FLIPL. J Cell Biol. 2010; 190: 377-389.
132. Ueffing N, Schuster M, Keil E, Schulze-Osthoff K and Schmitz I. Up-regulation of c-FLIP short by NFAT contributes to apoptosis resistance of short-term activated T cells. Blood. 2008; 112: 690-698.
133. Aurora AB, Biyashev D, Mirochnik Y, Zaichuk TA, Sanchez-Martinez C, Renault MA, Losordo D and Volpert OV. NF-kappaB balances vascular regression and angiogenesis via chromatin remodeling and NFAT displacement. Blood. 2010; 116: 475-484.
134. Apelbaum A, Yarden G, Warszawski S, Harari D and Schreiber G. Type I interferons induce apoptosis by balancing cFLIP and caspase-8 independent of death ligands. Mol Cell Biol. 2013; 33: 800-814.

135. Sun J, Luo H, Nie W, Xu X, Miao X, Huang F, Wu H and Jin X. Protective effect of RIP and c-FLIP in preventing liver cancer cell apoptosis induced by TRAIL. Int J Clin Exp Pathol. 2015; 8: 6519-6525.
136. Zhang YP, Kong QH, Huang Y, Wang GL and Chang KJ. Inhibition of c-FLIP by RNAi enhances sensitivity of the human osteogenic sarcoma cell line U2OS to TRAIL-induced apoptosis. Asian Pac J Cancer Prev. 2015; 16: 2251-2256.
137. Orzechowska E, Kozlowska E, Staron K and Trzcinska-Danielewicz J. Time schedule-dependent effect of the CK2 inhibitor TBB on PC-3 human prostate cancer cell viability. Oncol Rep. 2012; 27: 281-285.
138. Wang G, Ahmad KA and Ahmed K. Role of protein kinase CK2 in the regulation of tumor necrosis factor-related apoptosis inducing ligand-induced apoptosis in prostate cancer cells. Cancer Res. 2006; 66: 2242-2249.
139. Carcas LP. Gastric cancer review. J Carcinog. 2014; 13: 14.
140. Sasako M, Sakuramoto S, Katai H, Kinoshita T, Furukawa H, Yamaguchi T, Nashimoto A, Fujii M, Nakajima T and Ohashi Y. Five-year outcomes of a randomized phase III trial comparing adjuvant chemotherapy with S-1 versus surgery alone in stage II or III gastric cancer. J Clin Oncol. 2011; 29: 4387-4393.
141. Bang YJ, Kim YW, Yang HK, Chung HC, Park YK, Lee KH, Lee KW, Kim YH, Noh SI, Cho JY, Mok YJ, Kim YH, Ji J, Yeh TS, Button P, Sirzen F, et al. Adjuvant capecitabine and oxaliplatin for gastric cancer after D2 gastrectomy (CLASSIC): a phase 3 open-label, randomised controlled trial. Lancet. 2012; 379: 315-321.
142. Wieduwilt MJ and Moasser MM. The epidermal growth factor receptor family: biology driving targeted therapeutics. Cell Mol Life Sci. 2008; 65: 1566-1584.

143. Moasser MM. The oncogene HER2: its signaling and transforming functions and its role in human cancer pathogenesis. Oncogene. 2007; 26: 6469-6487.
144. Menard S, Pupa SM, Campiglio M and Tagliabue E. Biologic and therapeutic role of HER2 in cancer. Oncogene. 2003; 22: 6570-6578.
145. Tang D, Liu CY, Shen D, Fan S, Su X, Ye P, Gavine PR and Yin X. Assessment and prognostic analysis of EGFR, HER2, and HER3 protein expression in surgically resected gastric adenocarcinomas. Onco Targets Ther. 2015; 8: 7-14.
146. Bang YJ, Van Cutsem E, Feyereislova A, Chung HC, Shen L, Sawaki A, Lordick F, Ohtsu A, Omuro Y, Satoh T, Aprile G, Kulikov E, Hill J, Lehle M, Ruschoff J, Kang YK, et al. Trastuzumab in combination with chemotherapy versus chemotherapy alone for treatment of HER2-positive advanced gastric or gastro-oesophageal junction cancer (ToGA): a phase 3, open-label, randomised controlled trial. Lancet. 2010; 376: 687-697.
147. List T and Neri D. Immunocytokines: a review of molecules in clinical development for cancer therapy. Clin Pharmacol. 2013; 5: 29-45.
148. Young PA, Morrison SL and Timmerman JM. Antibody-cytokine fusion proteins for treatment of cancer: engineering cytokines for improved efficacy and safety. Semin Oncol. 2014; 4: 623-636.
149. Lee S and Margolin K. Cytokines in cancer immunotherapy. Cancers. 2011; 3: 3856-3893.
150. Penichet ML and Morrison SL. Antibody-cytokine fusion proteins for the therapy of cancer. J Immunol Methods. 2001; 248: 91-101.
151. Tarhini AA and Kirkwood JM. How much of a good thing? What duration for interferon alfa-2b adjuvant therapy? J Clin Oncol. 2012; 30: 3773-3776.

152. Tough DF, Borrow P and Sprent J. Induction of bystander T cell proliferation by viruses and type I interferon in vivo. Science. 1996; 272: 1947-1950.
153. Schiavoni G, Mattei F and Gabriele L. Type I Interferons as Stimulators of DC-Mediated Cross-Priming: Impact on Anti-Tumor Response. Front Immunol. 2013; 4: 483.
154. Herberman RB, Ortaldo JR, Rubinstein M and Pestka S. Augmentation of natural and antibody-dependent cell-mediated cytotoxicity by pure human leukocyte interferon. J Clin Immunol. 1981; 1: 149-153.
155. Balkwill F, Watling D and Taylor-Papadimitriou J. Inhibition by lymphoblastoid interferon of growth of cells derived from the human breast. Int J Cancer. 1978; 22: 258-265.
156. Cheon H, Borden EC and Stark GR. Interferons and their stimulated genes in the tumor microenvironment. Semin Oncol. 2014; 41: 156-173.
157. Pabari RM, Ryan B, Ahmad W and Ramtoola Z. Physical and structural stability of the monoclonal antibody, trastuzumab (Herceptin(R)), intravenous solutions. Curr Pharm Biotechnol. 2013; 14: 220-225.
158. AL R-W. Interferons: Production, Signaling and Uses in Cancer Treatment. Cutting Edge Therapies for Cancer in the 21st Century, 2014; p. 111-155.
159. Kim SJ, Park Y and Hong HJ. Antibody engineering for the development of therapeutic antibodies. Mol Cells. 2005; 20: 17-29.
160. Davis CB and Gillies SD. Immunocytokines: amplification of anti-cancer immunity. Cancer Immunol Immunother. 2003; 52: 297-308.
161. Jaitin DA, Roisman LC, Jaks E, Gavutis M, Piehler J, Van der Heyden J, Uze G and Schreiber G. Inquiring into the differential action of interferons (IFNs): an IFN-alpha2 mutant with enhanced affinity to IFNAR1 is

functionally similar to IFN-beta. Mol Cell Biol. 2006; 26: 1888-1897.
162. Yang CH, Wu PC, Huang YB and Tsai YH. A new approach for determining the stability of recombinant human epidermal growth factor by thermal Fourier transform infrared (FTIR) microspectroscopy. J Biomol Struct Dyn. 2004; 22: 101-110.
163. Naruse I, Fukumoto H, Saijo N and Nishio K. Enhanced anti-tumor effect of trastuzumab in combination with cisplatin. Jpn J Cancer Res. 2002; 93: 574-581.
164. Petricevic B, Laengle J, Singer J, Sachet M, Fazekas J, Steger G, Bartsch R, Jensen-Jarolim E and Bergmann M. Trastuzumab mediates antibody-dependent cell-mediated cytotoxicity and phagocytosis to the same extent in both adjuvant and metastatic HER2/neu breast cancer patients. J Transl Med. 2013; 11: 307.
165. Damdinsuren B, Nagano H, Wada H, Kondo M, Ota H, Nakamura M, Noda T, Natsag J, Yamamoto H, Doki Y, Umeshita K, Dono K, Nakamori S, Sakon M and Monden M. Stronger growth-inhibitory effect of interferon (IFN)-beta compared to IFN-alpha is mediated by IFN signaling pathway in hepatocellular carcinoma cells. Int J Oncol. 2007; 30: 201-208.
166. Rossi UA, Gil-Cardeza ML, Villaverde MS, Finocchiaro LM and Glikin GC. Interferon-beta gene transfer induces a strong cytotoxic bystander effect on melanoma cells. Biomed Pharmacother. 2015; 72: 44-51.
167. Llobet D, Eritja N, Encinas M, Llecha N, Yeramian A, Pallares J, Sorolla A, Gonzalez-Tallada FJ, Matias-Guiu X and Dolcet X. CK2 controls TRAIL and Fas sensitivity by regulating FLIP levels in endometrial carcinoma cells. Oncogene. 2008; 27: 2513-2524.
168. Schumacher TN and Schreiber RD. Neoantigens in cancer immunotherapy. Science. 2015; 348: 69-74.

국문 초록

인터페론 베타 기반 항암 치료법 연구

서울대학교 대학원
약학과 병태생리학 전공
김태은

인터페론 베타는 암세포에서의 세포사멸을 유도 가능하여 항암제로 관심을 받고 있다. 그러나 인터페론-베타에 대한 암세포 저항성과 이의 낮은 단백질 안정성, 투여 후 전신독성의 유발 가능성은 인터페론-베타의 항암제로서의 활용에 대한 제한을 가져왔다. 선행연구에서 본 연구그룹은 기존의 80번 아미노산에 N-glycosylation을 가지고 있는 재조합 인간 인터베론-베타1a (rhIFNβ-1a)의 27번 아미노산 Arginine을 Threonine으로 치환하여 25번째 아미노산에 추가 Glycosylation을 유도한 rhIFNβ-1a을 개발하였으며 R27T로 명명하였다. R27T는 기존의 rhIFNβ-1a와 비교하여 단백질 안정성과 체내 반감기가 향상된 것으로 나타났다. 그럼에도 불구하고, R27T를 항암제로 적용하기에는 저항성과

부작용 문제가 해결되어야 할 과제로 남아있다.

본 연구는 최초로 다양한 암세포주에서 R27T의 항암 효능에 대하여 시험하였으며, 내성 세포주에서 저하된 항-증식 및 세포사멸 효능이 R27T 처리에 의해 발현이 상승된 세포내 cellular FLICE-like inhibitory protein (cFLIP) 단백질이 Caspase의 활성을 저해하는 기전으로부터 유도됨을 확인하였으며 추가적으로 cFLIP의 저해가 R27T 내성세포에서 R27T에 의한 Caspase활성을 용이하게 하는 것을 관찰하였다. cFLIP siRNA 및 TBB (casein kinase-2 inbihitor)와 같은 cFLIP 저해제와 R27T의 병행요법이 *in vitro* 및 *in vivo*에서 R27T의 내성을 극복하는 전략으로 활용 가능함을 확인하였다.

본 연구는 R27T의 항암제로서의 활용을 위한 추가적인 전략으로 ERBB-2 양성 위암 환자의 치료를 목적으로 항-ERBB-2 치료용 항체인 trastuzumab에 R27T를 융합시킨 융합 단백질의 개발연구를 진행하였다. 항체의 C-term 말단에 재조합 단백질 기법을 활용하여 R27T를 융합하였으며, 본 융합단백질은 기존의 rhIFNβ-1a가 융합되었을 때보다 CHO 세포에서 높은 발현율을 보이는 것이 관찰되었다. 또한 Trastuzumab-R27T 융합단백질이 위암 세포주에서 인터페론 시그널을 정상적으로 유도할 수 있음을 확인하였으며, R27T 본래의 항암 효능도 온전히 보유하고 있는

것이 확인되었다. 더욱이 융합단백질은 trastuzumab과 비교하여 trastuzumab 본래의 antibody-dependent cellular cytotoxicity 효능을 정상적으로 보유하고 있음을 관찰하였다.

주요어: 재조합 인간 인터페론 베타-1a, R27T, 항암, 내성, cFLIP, trastuzumab, 융합 단백질

학 번: 2011-31101